

Final Report to U.S. Geological Survey

**Investigation of Structural Collapse Risk in the Cascadia
Subduction Zone**

Award Number: G11AP20134

PI: Abbie Liel

Dept. of Civil, Environmental and Architectural Engineering
University of Colorado, Boulder
Boulder, CO 80309
Email: abbie.liel@colorado.edu
Phone: (303)492-1050

Study Co-authored by: Meera Raghunandan,
Dept. of Civil, Environmental and Architectural Engineering
University of Colorado, Boulder
Boulder, CO 80309
Email: meera.raghunandan@colorado.edu

Term of Award: May, 2011 – April, 2013

This research was supported by the U. S. Geological Survey (USGS), Department of Interior, under award number G11AP20134. The views and conclusions contained in this document are those of the authors and should not be interpreted as necessarily representing the official policies, either expressed or implied, of the U. S. Government.

Table of Contents

OVERVIEW	2
 PART 1: EFFECT OF GROUND MOTION DURATION ON EARTHQUAKE-INDUCED STRUCTURAL COLLAPSE	 3
1. Introduction	3
2. Ground Motion Duration.....	4
3. Ground Motion Database	5
4. Building Design and Analytical Modeling	6
5. Nonlinear Analysis	9
6. Collapse Analysis Results	10
7. Does Duration Matter for Collapse Risk?	20
8. Conclusions	22
9. Acknowledgments	23
 PART 2: COLLAPSE RISK OF BUILDINGS IN THE PACIFIC NORTHWEST REGION DUE TO SUBDUCTION EARTHQUAKES.....	 28
1. Background and Motivation.....	28
2. Ground Motion Database	30
3. Seismic Design History	30
4. Archetype Building Designs and Models	33
5. Building Collapse Simulation	33
6. Collapse Results	36
7. Conclusions	43
8. Acknowledgements	47
9. References	47

Overview

This report describes the work done under grant number G11AP20134, entitled “Investigation of Structural Collapse Risk in the Cascadia Subduction Zone.” The report is presented in two parts. Part 1 investigates the influence of ground motion duration on structural collapse. Since subduction ground shaking tends to be of longer duration than crustal ground motions the investigation of ground motion duration was an important precursor to a broader investigation of structural collapse risk in subduction earthquake events. This part is reproduced from an article written by the same authors and published in *Structural Safety* in March, 2013 (<http://dx.doi.org/10.1016/j.strusafe.2012.12.002>). The second part of the completed research builds on part 1 and quantifies the collapse risk of existing and modern structures in the Pacific Northwest cities of Portland, Oregon and Seattle, Washington. The updated version of this report is reproduced from an article written by the same authors and accepted for publication in *Earthquake Spectra* in September, 2014.

A preliminary version of these results was presented at the USGS Workshop on Update of Pacific Northwest Portion of the U.S. National Seismic Hazard Maps held in Seattle, Washington in March, 2012.

Part 1: Effect of Ground Motion Duration on Earthquake-Induced Structural Collapse

1. Introduction

Earthquakes that have occurred in recent years, including those in Tohoku, Japan (M_w 9.0, 2011), Maule, Chile (M_w 8.8, 2010), and Sumatra, Indonesia (M_w 9.1, 2004), continue to remind us that very long duration ground shaking may occur at some sites [1]. In the Tohoku earthquake, sites across Japan experienced ground motions lasting for 40s to 270s [2], compared to, for example, ground motion durations on the order of 6s to 30s experienced in the Loma Prieta earthquake (M_w 6.93, 1989) [3]. Although the effect of shaking duration on structural damage is not always clear, reconnaissance teams investigating damage in past events have repeatedly attributed damage in some events and at some sites to long duration shaking, and the associated high number of load reversal cycles. Ground motions generated from large magnitude events, such as the recent earthquakes listed above, and recorded at sites situated some distance away from the epicenter, are particularly likely to be of long duration. The buildings constructed at these sites should therefore be capable of withstanding the expected long durations in addition to the expected ground motion intensities. Present building codes and analysis procedures are based on the probabilistic site-specific design spectra that do not directly consider duration [4].

It is well-known that ground motion duration and the number of cycles have an important influence on some types of earthquake damage, such as inducing liquefaction and slope instability [5,6]. Yet, there remains disagreement in the research community on the effect of ground motion duration on structural response [7]. For example, experimental studies of reinforced concrete and steel elements or frames have typically concluded that duration or number of cycles of loading is positively correlated to structural damage. The damage observed in connections of steel moment resisting frames in the Northridge and Kobe earthquakes was attributed to low cycle fatigue (*i.e.* many cycles). In addition, analytical studies adopting cumulative damage measures, like plastic strain, have generally found duration to be important in quantifying structural damage. However, analytical studies using maximum drift or displacement as a measure of damage in the structure contradict these findings, and generally have found no correlation between ground motion duration and increasing damage. Even in these types of studies, though, research employing structures with degrading characteristics and allowing for destabilizing effects of gravity loads shows that longer duration ground motions may in fact increase maximum structural responses. In summary, the relationship observed between ground motion duration and structural response is heavily dependent on the definition of ground motion duration and structural response parameter used and whether significantly nonlinear behavior and destabilization effects are considered [7].

This paper explores the influence of ground motion duration on structural collapse risk, which is a critical metric of life safety. Structural collapse occurs due to a combination of large amplitude demands (which past research suggests is not strongly duration dependent) and damage accumulated over multiple cycles during the earthquake (which past research indicates is significantly duration dependent). Previous studies have shown how ground motion intensity and frequency content affect structural collapse risk and failure mechanisms [8–11]. However, the influence of duration, or the number of cycles imposed on the structure, is not well understood. One possible hypothesis is that long duration motions impose larger energy demands on the structure and therefore may cause collapse at lower ground motion intensities. This hypothesis is supported by work by Ruiz-Garcia[12] and Iervolino *et al.*[13], which suggests that duration may be more important for collapse than other, more linear limit states, but it has not been directly explored. To further complicate matters, the ground motion duration itself is related to earthquake features like magnitude, distance to site, and fault type [14], so it is difficult to decouple the effects of duration from other earthquake and ground motion characteristics. Understanding the effect of ground

motion duration on structural collapse risk and failure mechanisms will bring us one step closer to preventing future earthquake-induced collapses.

This study quantifies the influence of ground motion duration on the predicted collapse response of concrete frame structures. Incremental dynamic analysis is carried out on a set of 17 archetypical reinforced concrete buildings representative of modern and older construction in high seismic regions of the U.S. Each of the analytical building models is subjected to a database of 76 ground motion time histories with varying duration. The simulations use nonlinear multiple-degree-of-freedom models, which are capable of capturing strength and stiffness deterioration, along with destabilizing effects of gravity loads. The collapse capacity of each structure is quantified by the median ground motion intensity causing collapse, measured in terms of inelastic spectral displacement. Once these results are obtained, the inelastic spectral displacement at collapse for all the buildings is studied as a function of duration, and the structure's fundamental (first-mode) period and ductility capacity using general linear modeling (GLM) regression techniques. In doing so, we expand on previous research by quantifying the correlation between duration and structural collapse resistance, which is a combined mechanism of different damage and response measures that have been studied independently before, utilizing nonlinear analysis models representing realistic building designs.

2. Ground Motion Duration

A ground motion time history or accelerogram, recorded from a particular earthquake at a particular site, can be characterized by a number of parameters including amplitude, frequency content, energy, and duration of shaking. There are many definitions for ground motion duration available in literature [15]. Bracketed duration considers the amplitude of the ground motion to measure the duration and is defined as the length of the time between which the absolute accelerogram exceeds some threshold acceleration (*e.g.* 0.1g) for the first and last time. The significant duration, on the other hand, is defined based on the energy of the ground motion record. Several measures serve as proxies for the total energy of the accelerogram, including the integral of the square of the acceleration history over time $a(t)$, which is known as the Arias intensity (AI) and is calculated as

$$AI = \frac{\pi}{2g} \int_0^{T_r} a^2(t) dt \quad (2.1)$$

where T_r is the total recorded time of the accelerogram and g is the acceleration due to gravity. Among the different definitions of significant duration present in the literature, the 5-95% significant duration [16] is employed here, as it has been used and recommended by a number of other studies [7,17]. The 5-95% significant duration, denoted 5-95% D_s , is calculated as the interval between the times at which 5% and 95% of the Arias Intensity of the ground motion have been recorded, representing the duration of time over which 90% of the energy is accumulated. Although the total length of the accelerogram may vary depending on the recording device, the 5-95% D_s quantifies the length of the strongest part of the ground motion time history, *i.e.* that part of the motion which may damage a structure. This duration definition is also independent of the scaling of the record, as the rate of accumulation stays the same, and also does not vary with ground motion frequency content. Fig. 1 shows two recorded ground motions having the same peak ground accelerations (PGA), but different durations. The Arias Intensity plot (Fig. 1b) shows that the energy accumulates over more time for the longer duration ground motion as compared to the shorter duration ground motion. The time histories in Fig. 1a also illustrate the greater number of load reversal cycles for the longer duration record.

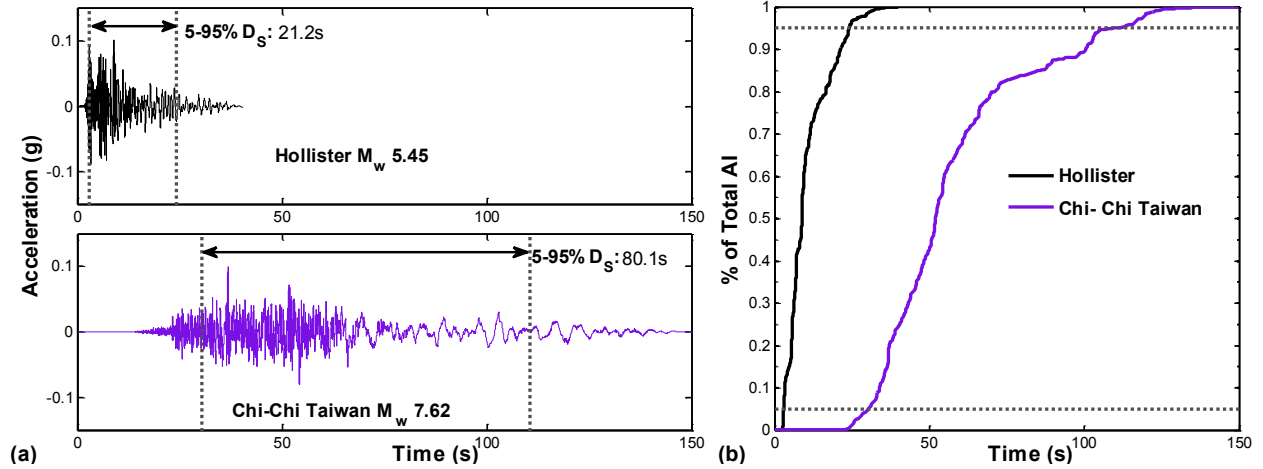


Fig. 1 (a) Ground acceleration time histories and (b) Arias intensity for Hollister (NGA Sequence Number: NGA0498) and Chi-Chi Taiwan (NGA1181) ground motion recordings with the same peak ground acceleration (PGA), but different durations.

3. Ground Motion Database

To consider a broad range of ground motion duration values, 76 ground motion records with 5-95% D_s varying between 1.1s to 271.3s are used in the dynamic analysis. The distribution of duration values in the record set is illustrated in Fig. 2a. Details of the records are provided in Appendix A. These ground motion records are obtained from the Pacific Earthquake Engineering Research Center (PEER) Next Generation Attenuation database [3], the COSMOS virtual data center[18], and the USGS National Strong-Motion Project [19]. The records are from 24 different earthquakes with M_w 4.8 and above, with the maximum number of the records from a single event being limited to eight. Due to lack of availability of recordings for large long duration ground motions, particularly those from potentially large magnitude subduction events, this study also uses eight simulated records from Yang [20], in addition to the 68 strong motion recordings. Among short duration records, of which there are many ground motion recordings available, records with the largest $PGAs$ were selected. To avoid any near site effects or effects of rupture directivity, only ground motions without large pulses in the velocity time history are used in dynamic analysis [21]. The record selection process did not consider spectral shape, but this is not expected to have a critical influence on the fragility predictions, due to the use of an inelastic ground motion intensity measure (described later in Section 5).

The significant duration of a ground motion at a site depends on various factors, such as earthquake moment magnitude, distance to the fault rupture, depth to the top of rupture, soil type and the type of earthquake [14]. Seismological theory and models predict that duration of shaking at the source increases with an increase in seismic moment or earthquake magnitude [22]. As the magnitude of the earthquake increases, so does the length and area of the fault rupture, which increases the time taken for the strain energy to release, resulting in longer strong motion durations at the source. The ground shaking duration modifies further as waves travel to a particular site, due to the factors such as soil and distance [14]. In general, as seismic waves scatter with distance between the source and site, the duration of ground shaking tends to become larger because of the increased difference in time between the arrivals of different seismic waves. Ground motion recordings from soil sites usually exhibit longer durations than rock sites [14].

This study uses ground motion records from crustal and subduction events (M_w 4.8 - M_w 9.2), and the increase in duration with magnitude for these ground motions can be seen clearly in Fig. 2b. The relationship between site epicentral distances and duration is also apparent in the record set, as shown in

Fig. 2c. Record $PGAs$ vary between 0.02g and 0.73g. Fig. 2d shows that most of the long duration records have low PGA because they are recorded at large distances from the source, and seismic wave amplitudes have attenuated significantly [14]. Long duration records also may have differences in frequency content and response spectra shape from shorter duration records [23]; this issue is addressed in further detail in the discussion of ground motion intensity measures in Section 5. The database ground motion recordings are mostly for stiff soil and rock sites.

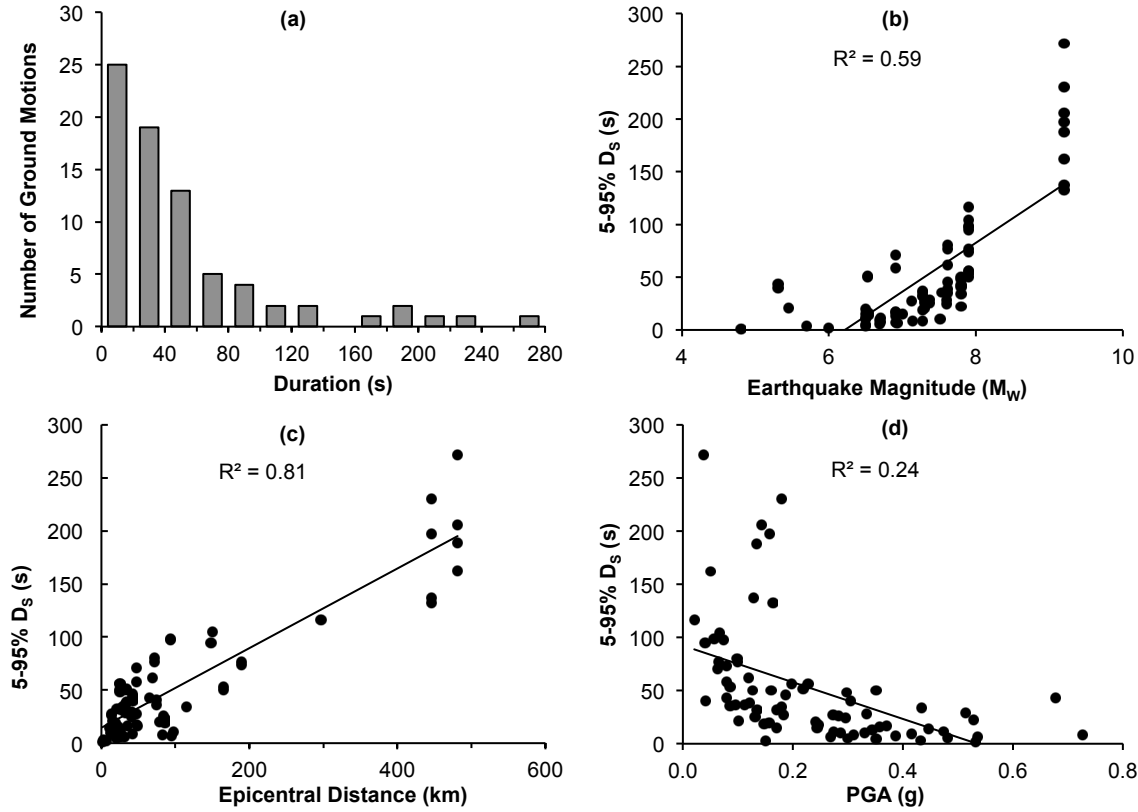


Fig. 2 Distribution of ground motions in database according to (a) duration, (b) moment magnitude (M_w), (c) epicentral distance and (d) PGA

4. Building Design and Analytical Modeling

To assess the effect of the ground motion duration on the collapse of structures, nonlinear dynamic analysis is conducted for 17 archetypical reinforced concrete building models designed and detailed according to the requirements of past and present U.S. seismic codes. The use of this wide array of building models, which vary in terms of the fundamental period, ductility capacity and other key properties, enables us to quantify the influence of ground motion duration on the response of buildings with different structural properties.

The buildings in this study can be broadly classified into two categories: (a) modern ductile reinforced concrete frames and (b) older non-ductile reinforced concrete frames. It is meaningful to consider modern-type ductile buildings because current seismic codes do not directly address ground motion duration in design. The inclusion of non-ductile concrete frame buildings is important because these structures are prevalent in high seismic regions worldwide, and may be particularly vulnerable to earthquake-induced collapse [24]. The modern ductile frames are designed by Haselton *et al.*[11] according to the provisions of the International Building Code [25], ASCE 7-05 [26], and ACI 318-02

[27]. These buildings satisfy all the requirements of so-called “special” moment resisting reinforced concrete frames, including strong-column-weak-beam requirements, shear capacity design and detailing requirements. The group of non-ductile buildings is designed by Liel *et al.*[24] in accordance with Uniform Building Code [28] for the highest seismic zone at that time (*i.e.* California). These frames have somewhat lower strength and significantly lower deformability than the modern frames of comparable height. In particular, the low quantity and poor detailing of transverse reinforcement in structural elements and joints makes them susceptible to brittle failure modes. Table 1 provides the height, framing system (space or perimeter frame type) and other design details for each building. The last column in Table 1, μ_T , provides one measure of the building ductility capacity, or the amount of inelastic deformation the structure can undergo, as obtained from static pushover analysis. Note that there are other measures of building ductility capacity, but this pushover-based measure defined by FEMA P695 [29] is used here to quantify relative differences in building deformability. Additional documentation of building design and modeling can be found in Haselton *et al.*[11] and Liel *et al.*[24].

Table 1 Building Design Information

ID ^[a]	T_1 ^[b] (s)	Design Base Shear Coefficient ^[c]	μ_T ^[d]
02MS	0.60	0.125	15.9
04MP	1.08	0.092	11.5
04MS	0.91	0.092	12.4
08MP	1.69	0.050	10.3
08MS	1.81	0.050	7.7
12MP	1.97	0.044	13.0
12MS	2.15	0.044	7.3
20MP	2.59	0.044	9.1
20MS	2.53	0.044	9.6
02OS	1.03	0.086	3.4
02OP	1.00	0.086	8.0
04OP	1.89	0.068	2.7
04OS	1.92	0.068	2.4
08OP	2.33	0.054	2.2
08OS	2.23	0.054	2.6
12OP	2.73	0.047	2.1
12OS	2.35	0.047	2.9

^[a] Building information provided in ID: First two characters indicate the number of floors; third character “O” denotes older design and “M” denotes modern design; last character indicates “S” for space frame and “P” for perimeter frame.

^[b] First-mode elastic (fundamental) structural period based on eigenvalue analysis, considering cracked concrete sections.

^[c] Ratio of the design base shear to the building weight (V_{design}/W).

^[d] Ductility capacity as determined by nonlinear static pushover analysis.

The archetypical buildings are modeled as two-dimensional, three-bay frames of varying height, as shown in Fig. 3. These models are implemented in OpenSees [30], an open-source, object-oriented software platform developed by PEER. In order to simulate structural response up to the point of structural collapse, the nonlinear analytical models must be capable of capturing important modes of deterioration and failure. Accordingly, a model comprised of lumped plasticity beam-column elements and inelastic joint shear springs has been used to represent the flexural behavior of beams and columns and joint shear failure. The plastic hinges in the lumped plasticity beam-column element are modeled using the hysteretic material developed by Ibarra *et al.*[9], which is capable of simulating stiffness and strength degrading hysteresis behavior of the beams and columns as the structure collapses. Examples of the tri-linear monotonic backbone curve and the hysteretic behavior of the element hinges and joint springs are provided in Fig. 4. The plastic hinges’ negative post-capping stiffness represents strain softening response caused by spalling of cover concrete and buckling of longitudinal reinforcing bars. Model parameters for

beam-column hinges are determined from the empirical equations obtained by calibrating the Ibarra hysteresis model to more than 250 experimental tests of concrete columns [31]. Therefore, model properties such as rotation capacity and post-capping stiffness vary according to the design and detailing properties of each frame and beam or column. A key parameter from the perspective of this study is the cyclic deterioration, which is modeled in each hinge by a parameter λ that represents the cyclic hysteretic energy dissipation capacity of the element [9]. The values of λ have been calibrated to experimental data such that more ductile well-detailed columns and beams have higher λ , indicating that the element is able to dissipate more energy and has a lower rate of strength and stiffness deterioration [31]. Prediction of column shear failure and loss of gravity load bearing capacity in dynamic analysis is progressing with newly developed computational models [32,33], but is not considered in this study and models do not capture shear critical column response. The modern building columns are designed to prevent this failure mode through capacity design provisions of transverse reinforcement. In the older buildings, columns are assumed to display flexure-shear failure, *i.e.* yielding before shear failure occurs. Foundation flexibility is modeled with an elastic, semi-rigid rotational spring at the base of each column. Destabilizing P- Δ effects are incorporated using a nonlinear geometric transformation. In addition, a leaning column of truss elements is connected to the frame by rigid struts (Fig. 3). The load, P , on the leaning column includes the gravity loads that are not tributary to the modeled 2-dimensional frame.

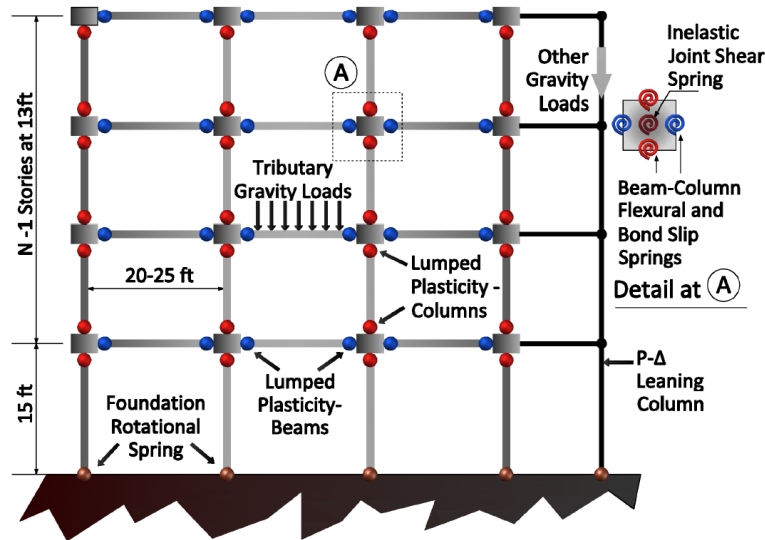


Fig. 3 Schematic of N-story building model showing key nonlinear elements used for dynamic analysis

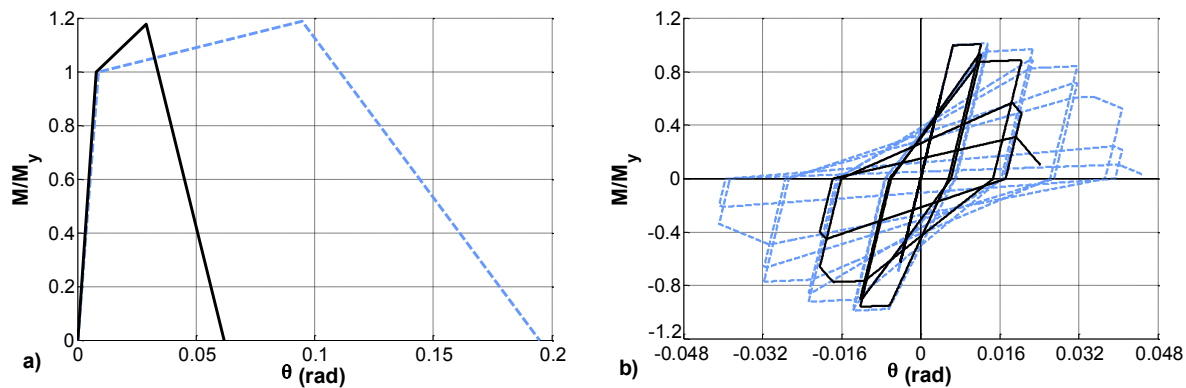


Fig. 4 Properties of component model for the typical ductile (dashed) and non-ductile (solid) reinforced concrete columns, illustrating differences in (a) monotonic and (b) cyclic behavior [24].

5. Nonlinear Analysis

The seismic response of the building model is evaluated using incremental dynamic analysis (IDA) [34]. In IDA, a nonlinear building model is subjected to a ground motion with a particular intensity, and the time history of building response, including key engineering demand parameters such as peak interstory drift, roof drift, or floor acceleration, are measured. The ground motion record is then scaled to increasing intensity and dynamic analysis is repeated. This procedure of scaling and time history analysis is repeated until dynamic instability in the form of large interstory drifts occurs, indicating building collapse. The severity of the ground motion is quantified using an intensity measure such as PGA or $S_a(T_1)$, the spectral acceleration at the first-mode period of the building. Scaling of records is needed to simulate the behavior of the structure to varying levels of seismic demand, providing insight into how the structure might respond under rare large intensity ground motions, for which few or no recordings are available. To account for record-to-record variability in frequency content and other ground motion features, the analysis is conducted for a suite of different ground motions.

Recent research has shown that, in addition to the ground motion intensity, the spectral shape of ground motions affects inelastic structural response [35]. The intensity measure conventionally used in building fragility analysis, $S_a(T_1)$, does not account for the spectral shape of the ground motion record because it represents the response spectral value only at a single period, usually the fundamental period of the structure. In particular, $S_a(T_1)$ does not capture period elongation and higher mode effects, such that different ground motions with the same $S_a(T_1)$, but different shapes, may affect highly nonlinear multiple degree of freedom structures differently. This observation is significant because rare ground motions that are large enough to cause collapse have a distinct shape [35]. Other intensity measures, such as peak ground velocity (PGV), which is correlated to the failure of long period structures, suffers from a similar deficiency because it does not cover the wide range of frequencies required to adequately capture the spectral shape of the ground motion recording [36]. The use of inelastic spectral displacement, or S_{di} , as an intensity measure, has been shown to be effective in representing both ground motion intensity and the spectral shape effect [37].

Inelastic spectral displacement is calculated as the maximum (spectral) displacement of a single-degree-of-freedom oscillator with bilinear material properties [38]. S_{di} is typically calculated for 5% damping, and depends on the specified first-mode elastic period and the yield displacement of the oscillator, d_y (Fig. 5a). In this study, d_y is obtained from nonlinear pushover analysis of building model and is structure-specific [29]. The bilinear oscillator is assumed to have a 5% post-yield hardening stiffness ratio and is infinitely ductile. The shape of the response spectra for periods greater than the oscillator's fundamental period is implicitly captured by S_{di} , due to the oscillator yielding and elongation of the oscillator period [38]. Because S_{di} accounts for spectral shape variability as well as ground motion intensity, its use reduces record-to-record variability in structural response as compared to other intensity measures [12]. S_{di} does not account for the portion of the spectra where periods are shorter than the first-mode period, which may influence higher modes. Nevertheless, this study uses S_{di} as an intensity measure due to its simplicity and at the same time its suitability in accounting for the most important issues related to spectral shape, since higher modes are not critical for the building set of interest. Since long duration records tend to have different frequency content than their short duration counterpart because of the type of rupture and wave path effects [23], the use of S_{di} is particularly important here, because it allows us to focus on ground motion duration distinct from spectral shape issues. Also, if S_{di} is used, structural response results have been shown to be unbiased by the scale factor applied to the record before the analysis[37].

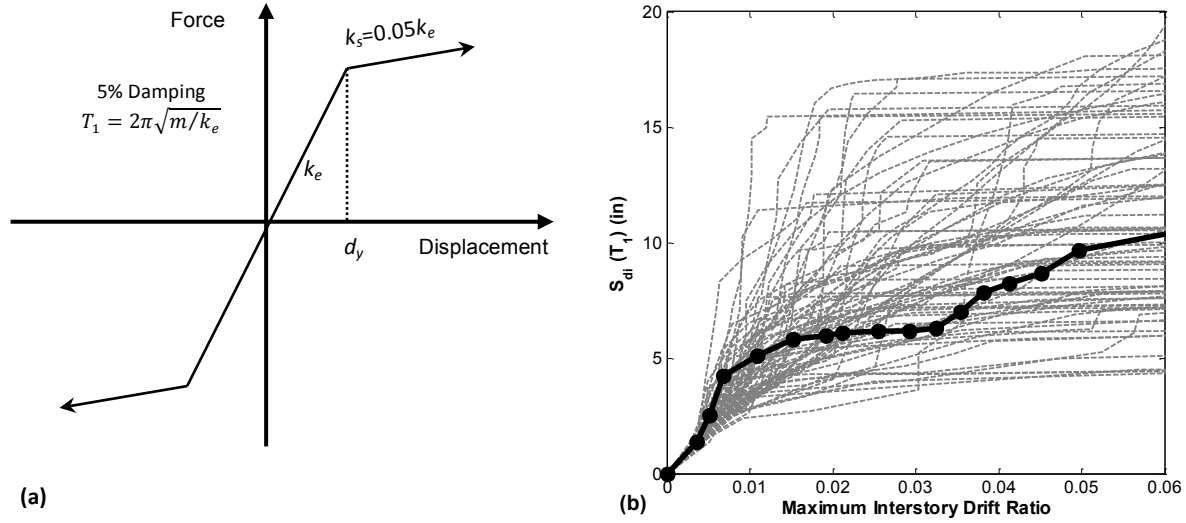


Fig. 5 (a) Properties of the single-degree-of-freedom oscillator used in calculation of inelastic spectral displacement, S_{di} , (b) Incremental dynamic analysis results for the 4-story modern reinforced concrete building (04MP).

IDA results for the 4-story modern reinforced concrete space frame (04MP) are shown in Fig. 5b, where, the interstory drifts are plotted for increasing levels of inelastic spectral displacement for 76 different ground motions. The black line highlights IDA results for one of the ground motion time histories, describing the trends in the maximum interstory drift of the structure as it is subjected to increasing intensities of same ground motion. The results for the other ground motions are shown in gray.

6. Collapse Analysis Results

6.1 Overview

The collapse capacity of a structure is quantified by a ground motion's inelastic spectral displacement when it is scaled to level at which structural collapse occurs. A larger value of S_{di} at collapse (for a particular building period and d_y) indicates that the structure is able to withstand larger ground motion intensities before the collapsing. To quantify the influence of ground motion duration on the collapse capacity of a structure, a multivariate regression model is fitted to structural analysis results from all buildings using the generalized linear model (GLM) framework [39]. In the process of finding the best-fit GLM model, the influence of various building properties (*e.g.* fundamental period, ductility or deformation capacity, and lateral load resisting system) and ground motion properties (*e.g.* peak ground acceleration and significant duration) on the collapse S_{di} is considered. Fig. 6 shows the relationship between collapse S_{di} and duration for four different buildings, where each marker indicates the collapse S_{di} value recorded for one of the 76 ground motion records and the curves represent the fitted GLM models. Results for all the buildings show a decrease in collapse S_{di} with increasing ground motion duration.

In Fig. 6, and the discussion below, the best GLM model fitted to the data from all buildings, the so-called “common” or “final” model, indicates that the collapse capacity of a structure depends on its ductile or non-ductile nature and its fundamental period, along with the duration of the ground motion to which it is subjected. The curve labeled “individual building model” has been fitted only to the results from that particular building model. The development of the GLM model and the functional form is discussed in more detail in the following sections.

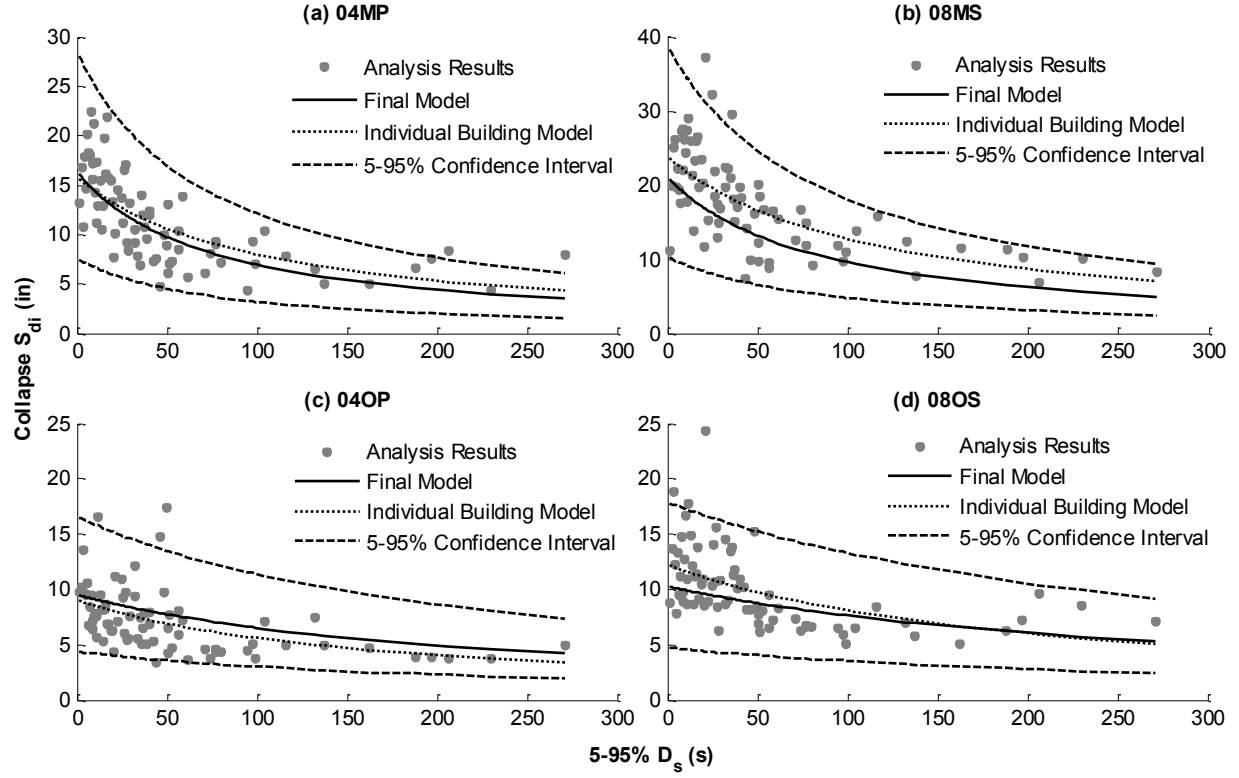


Fig. 6 Variation of Collapse S_{di} with Ground Motion Duration for (a) Modern 4-Story building, (b) Modern 8-Story Building, (c) Older 4-Story Building, and (d) Older 8-Story Building.

6.2 Statistical Analysis of Collapse Results

The structural collapse capacity variable, S_{di} , is modeled using GLM as a function of two structural parameters, the building's fundamental period (T_1) and its ductility capacity, and a ground motion duration parameter (5-95% D_S). Building ductility capacity is included in the model by assigning building ductility flag values of $B_F = 1$ for the modern ductile buildings and $B_F = 2$ for the older non-ductile buildings. We also computed building-specific structural ductility capacity parameters from nonlinear pushover analysis (reported in Table 1) as possible predictors for preliminary GLM models, but the flag variable distinguishing simply between those buildings that are quite ductile (quantitatively representing ductility values obtained from pushover analysis with $\mu_T \geq 7$) and those that are not ($\mu_T \leq 7$) was found to be a more significant predictor collapse S_{di} than the building-specific values.

Mathematically, the GLM model can be expressed as:

$$S_{di} = f(T_1, B_F, D_S) + error \quad (6.1)$$

GLMs are a general form of the linear regression models. In linear regression modeling, the vector of response variables, Y (in our case, collapse S_{di}), is expressed as a linear combination of n predictor variables, $X = [1, x_1, x_2, \dots, x_n]$ (in our case, $x_1 = T_1$, $x_2 = B_F$ and $x_3 = D_S$):

$$Y = X^T \beta + error \quad (6.2)$$

β is the $(1+n) \times 1$ vector of estimated model parameters (*i.e.* regression coefficients) for the predictor variables X . A linear least-squares regression model is appropriate for a continuous response variable, Y , which is normally distributed with constant variance, but is not suitable for other Y . In GLM, the distribution of Y may follow any exponential family distribution whose parameters can be varied to represent both discrete (*e.g.* binomial, Poisson) and continuous (*e.g.* normal, gamma) probability distributions. The GLM methodology also introduces a linearizing link function $g(\cdot)$ which is a one-on-one continuous differentiable transformation between the expectation of the response variable $E(Y)$ and the linear predictor $X^T \beta$.

$$g(E[Y]) = X^T \beta \quad (6.3)$$

The expected value of Y predicted using GLM is therefore calculated as:

$$E[Y] = g^{-1}(X^T \beta) \quad (6.4)$$

The link function varies for different distributions of Y . The typical linear regression model is a special case of GLM where Y has a normal distribution and the link function is the identity function.

In this study, the response variable values of $Y = S_{di}$ are assumed to follow a gamma distribution. The gamma distribution is capable of mimicking the shape of the lognormal or the exponential distribution by varying its parameters. This property makes the gamma distribution a good choice for S_{di} because collapse capacities are continuous and positive, and are typically assumed to follow a lognormal distribution. The gamma distribution requires a simple reciprocal (inverse) link function to define the relationship between the linear predictors and response variable such that:

$$E[S_{di}] = g^{-1}(X^T \beta) = \frac{1}{X^T \beta} \quad (6.5)$$

This inverse link function captures the nonlinear variation of S_{di} with respect to its predictor variables. The gamma distribution is defined by a shape parameter, which controls the skewness of the distribution, and a scale parameter, which is related to the spread of the distribution [40]. To calculate the expected value (mean) of the response parameter, the GLM methodology uses a constant shape parameter and scale parameters changing across the predictor variables to capture the variation in the variance of data. When the shape parameter is constant, the gamma distribution has a non-constant variance that is directly proportional to the square of the mean.

The GLM modeling is carried out using the *glm* package in *R* [41], which estimates the model parameters by an iterative procedure that maximizes the likelihood function to determine the most probable parameter values for the given observed data. The GLM model is fitted for different combinations of one, two or three of the predictor variables T_I , B_F and D_S and multiplicative interaction variables (*e.g.* $T_I \times B_F$) between them. The analysis is carried out on a single matrix for all 17 buildings and all 76 ground motions with a 1292×1 S_{di} vector as the response variable and a $1292 \times (1 \text{ or } 2 \dots \text{ or } 6)$ predictor variable matrix X . The predicted residual sum of squares (PRESS) for each model is calculated and the “best” model is defined by the predictors and coefficients, β , which minimize the PRESS (Predicted REsidual Sums of Squares) score [42]. The fitted GLM model, reported in Equation 6.6, shows that all

three predictors and an interaction term between D_s and T_1 are important. For comparison, separate GLM models were also fit to the data from each of the 17 buildings individually, and labeled as “Individual building model” in Fig. 6.

$$E[S_{di}](in) = \left[\frac{1}{\left(2.33 \times 10^{-2} + 1.29 \times 10^{-3} * D_s - 2.23 \times 10^{-2} * T_1 \right) - 4.28 \times 10^{-4} * D_s * T_1 + 6.19 \times 10^{-2} * B_F} \right] \quad (6.6)$$

The confidence intervals for the final model prediction can be obtained by calculating the 5 and 95% quantiles of the gamma distribution about each estimated response value (mean) with the shape and scale parameter values at that point. The confidence intervals were computed in the *glm* package in R and are illustrated for 4 typical buildings in Fig. 6.

There are a variety of other measures of goodness of fit in the context of GLM. Analysis of Variance (ANOVA) is carried out on the final model predictors (β), testing the statistical significance of each model parameter, which are themselves random variables. Table 2 summarizes the β values along with their standard error used in hypothesis testing. The null hypothesis stating that all coefficients β are zero can be rejected for all the predictors that have p value less than the significance value, $\alpha = 5\%$. The ANOVA results are summarized in Table 2 with p values extremely close to zero, indicating that the null hypothesis can be rejected and that each of the selected predictors is important.

Table 2 “Best” Model Parameters

Model Parameter	β	Standard Error	p value
Intercept	2.33×10^{-2}	4.34×10^{-3}	9.2×10^{-8}
Duration, D_s	1.29×10^{-3}	8.59×10^{-5}	$<10^{-16}$
Fundamental Period, T_1	-2.23×10^{-2}	1.70×10^{-3}	$<10^{-16}$
$D_s \times T_1$	-4.27×10^{-4}	3.78×10^{-5}	$<10^{-16}$
Building Ductility Flag, B_F	6.18×10^{-2}	1.86×10^{-3}	$<10^{-16}$

The S_{di} estimates calculated according to Equation (6.6) have been shown for selected buildings in Fig. 6 and are plotted against the actual values obtained from nonlinear analysis in Fig. 7a. For a model that perfectly predicts the response variable, the estimated values from the GLM model would be the same as the actual values, falling on the 45° line. The GLM model follows this trend, with dispersion around 45° line representing the uncertainty in the prediction. To check the robustness of the chosen “best” GLM model, a cross-validation procedure is carried out. In cross-validation, a subset of the data is dropped from the original dataset and the GLM model is fitted to the remaining data (referred to hereafter as the “reduced model”). The reduced model is then used to predict values for the dropped subset of data. The robustness of the model is evaluated by its ability to predict values the reduced dataset has not seen before (*i.e.* the dropped values). Typically, around 10% of the data is dropped. In this study, the 76 observations associated with one building are dropped at a time. Fig. 7b shows that results from the reduced models results also follow the expected 45° line. In Fig. 7c, the cross-validated and estimated S_{di} values are very similar.

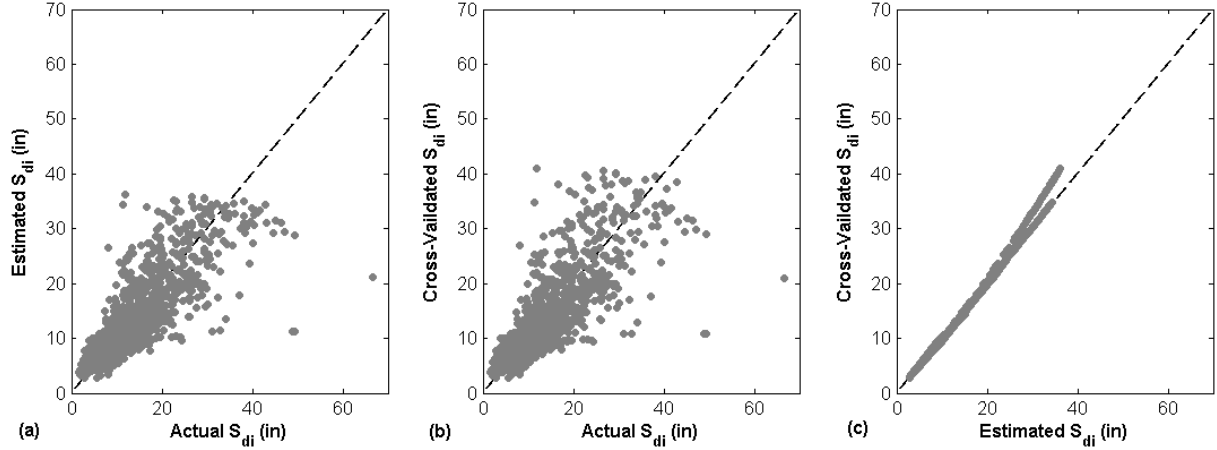


Fig. 7 Comparison of the selected “best” GLM model and cross-validated GLM models with collapse S_{di} from nonlinear analysis (“Actual S_{di} ”) for all buildings

The “best” GLM model illustrated in Fig. 8 shows variation in collapse $E[S_{di}]$ values with ground motion duration (5-95% D_s) and the fundamental period of structure (T_l) for the two subsets of buildings with different ductility capacities. The figure illustrates a clear decrease in collapse capacity with increase in duration for both ductile and non-ductile buildings. For example, for ductile and non-ductile buildings with $T_l=1$ s, there will be a 23% and 15% decrease, respectively, in mean collapse capacity on being subjected to a ground motion record having 5-95% D_s of 60s instead of a record having 5-95% D_s of 30s. The longer duration ground motions require a structure to undergo a larger number of load reversal cycles, resulting in higher accumulation of damage and higher imposed energy demands at lower levels of ground motion intensity. This behavior is examined in more detail in Sections 6.3.2 and 6.3.3. Fig. 8 further illustrates, unsurprisingly, that the modern buildings, which are designed and detailed to be ductile, have higher S_{di} collapse capacities than the non-ductile buildings regardless of 5-95% D_s and T_l . As shown many times before (*e.g.* Liel *et al.*[24], Ibarra *et al.* [9]), structures with higher ductility capacity are able to deform more before collapsing, resulting in more energy dissipation, and enabling them to withstand higher amplitudes of shaking before collapsing. The difference in collapse capacities of ductile and non-ductile buildings reduces as the ground motion duration increases, because the rate of decrease of collapse capacity with duration is higher for ductile buildings, as discussed in more detail in Sec 6.3.3. Fig. 8 also shows that an increase in T_l is associated with an increase in collapse S_{di} values. The effect of the fundamental period T_l on the collapse S_{di} can be explained by the shape of inelastic displacement spectrum. Like the elastic displacement spectrum, inelastic spectral displacement for a particular ground motion tends to increase with longer building periods so this trend reflects the average shape of the spectra.

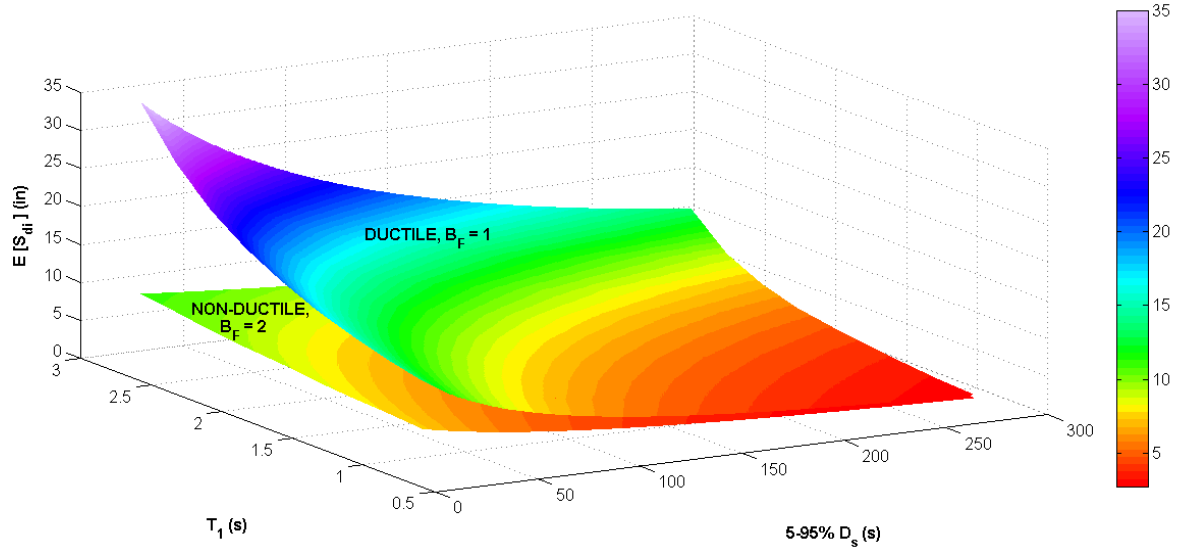


Fig. 8 Variation of $E[S_{di}]$ with 5-95% D_s and T_1 from the final GLM Model

6.3 Duration's Effect on Structural Collapse

The GLM model indicates that the collapse capacity of the structure is significantly affected by the duration of ground motion to which it is subjected. This section attempts to explicate the trends observed in the statistical analysis and to assess how variation in ground motion duration leads to differences in structural response.

6.3.1 Interstory and Residual Drift Demands

The time histories of interstory drift ratios and residual interstory drift ratios are two of the structural response parameters measured during the nonlinear dynamic analysis. Fig. 9 shows the variation of maximum interstory drift (*i.e.* the peak transient drift in the building, considering all stories) during the time history, and maximum residual interstory drift at the end of analysis for the 4-story modern building (04MP) for all ground motion records, scaled to three different ground motion intensity levels. There is essentially no trend observed between the maximum interstory drifts or residual drifts and duration, at ground motion intensities of $S_{di} = 2.25$ in. (building undergoing linear behavior) and 7.5 in (building undergoing nonlinear behavior). (Fig. 9a-d). (For reference, the range of collapse S_{di} for 04MP building is 4.3-22.4 inches with around 21% of the records having collapse S_{di} less than 7.5 in.) This observation agrees with Hancock and Bommer's [7] review of literature, which showed no relationship between duration and drift demands. In Fig. 9e-f, results are plotted for each record for the ground motion intensity level just below the intensity level at which collapse occurs. Since each record collapses at a different level, the intensity of each of the ground motions in these figures is different. These results show a slight decrease in drifts as the duration of ground motion increases. This general decrease in drift values, although a bit scattered, is because the longer duration records are likely scaled to lower intensities because, as shown earlier, they cause collapse at lower ground motion intensities. According to the results shown in Fig. 9 and similar observations for the other buildings, longer duration ground motion does not seem to lead to larger interstory or residual drifts in buildings, and hence, these drifts do not appear to be the explanation for why collapse occurs at lower ground motion intensities when subjected to the longer duration records.

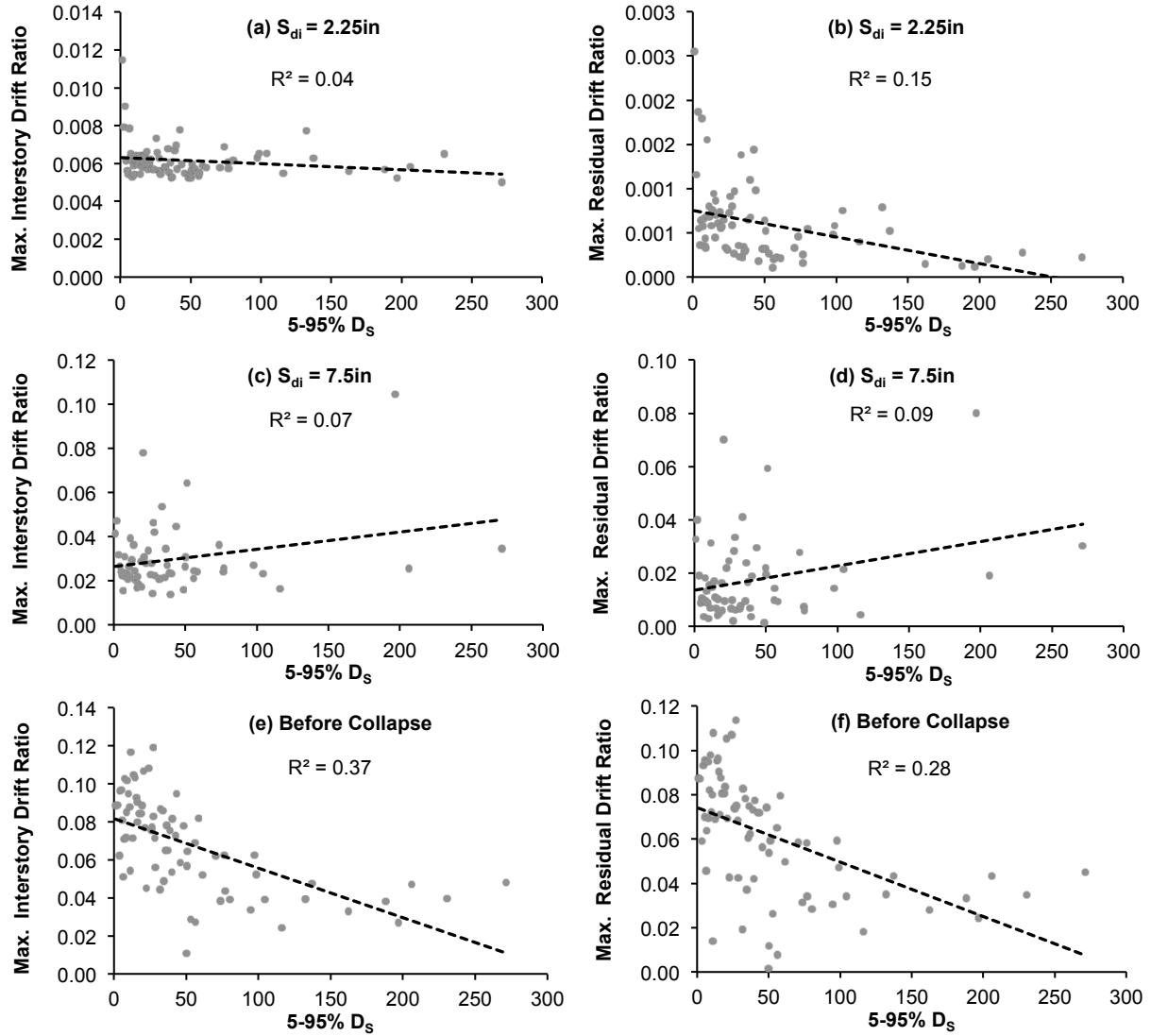


Fig. 9 Variation of max. interstory drift and max. residual interstory drift when all ground motions are scaled to intensities of $S_{di}=2.25 \text{ in.}$ and 7.5 in. for the modern 4-story building (04MP). In (e) and (f) each ground motion is scaled to the intensity just below that causing collapse.

6.3.2 Hysteretic Energy Demand

To interrogate the differences in structural response under longer and shorter duration ground motions, the total hysteretic energy dissipated by a structure as it deforms on being subjected to each ground motion is calculated. During the course of ground shaking, seismic energy is transferred to the structure where it takes the form of kinetic energy or elastic strain energy, or is dissipated through damping and hysteretic behavior [43]. Hysteretic energy can be used to represent the energy dissipated by the structure or, alternatively, the energy demand on the structure on being subjected to a dynamic force having load reversal cycles such as an earthquake.

The hysteresis energy dissipated by the structure is equal to the area inside the hysteresis loop, which can be expressed in various ways: bending moment versus rotation, story shear versus lateral displacement, or axial forces versus axial displacements etc. For the purpose of this analysis, the hysteretic energy

dissipated at each story over the duration of ground shaking is calculated as the area enclosed by the hysteresis loop formed by the earthquake-induced story shear forces and the relative displacement between floors at each story. The total hysteresis energy is calculated as the sum of hysteretic energy dissipated for all stories over the course of a particular ground motion time history.

$$\text{Total Hysteretic Energy, } E_H = \sum_{i=1}^N \sum_{j=1}^n E_{j,i,H} \quad (6.7)$$

Here, $E_{j,i,H}$ is hysteresis energy dissipated in the j^{th} cycle at the i^{th} story, n refers to the number of cycles in structural response and N is the total number of stories.

The total hysteresis energy calculated considers both elastic and inelastic displacements and so represents the sum of the elastic strain energy and inelastic hysteretic energy. [43] proposed that the inelastic part of the energy dissipation of structure can be represented by a ductility factor based on total hysteresis energy, μ_E , which is defined as the ratio of total hysteresis energy to the elastic strain energy. In this formulation, the elastic strain energy is calculated as $0.5 \times F_y \times d_y$, where F_y and d_y are the load and displacement at first yield. Accordingly, the trends observed between total hysteresis energy, E_H , and ground motion duration will be the same as the trends between μ_E and ground motion duration for a building having a particular F_y and d_y . Therefore, we use the total hysteresis energy as a simple and efficient parameter for the examining variability in inelastic energy dissipation by a particular structure on being subjected to different duration ground motions.

The total hysteretic energy dissipated by the 04MP building model for different duration ground motions at different S_{di} levels is shown in Fig. 10. More energy is dissipated by the system on being subjected to long duration ground motions in comparison to short duration ground motions at a particular ground motion intensity, as captured by the simple linear regression in Fig. 10a-b. The greater energy demand from the long duration records for a given ground motion intensity level can be attributed to the larger number of cycles. The effect of the number of cycles becomes more significant at higher intensity levels, with greater inelastic deformations, as seen by the increase in regression line slope between Fig. 10a and b. Fig. 10c shows the energy dissipated at the scale level just below that at which collapse occurs; the total energy dissipated at the intensity level just before collapse increases slightly with increasing duration. If the trendline were completely flat, the analysis would indicate that the same amount of energy demand is required to collapse the structure, regardless of duration. However, the longer ground motions, which are scaled to lower intensity levels, actually impose more energy demands on the structure compared to shorter duration records before collapse occurs, as indicated by the positive trend in Fig. 10c. For a given imposed energy demand, short duration ground motions may be more damaging, in part because of pulse effects [44], although we did not investigate this directly in our study. Similar results were observed for the other buildings.

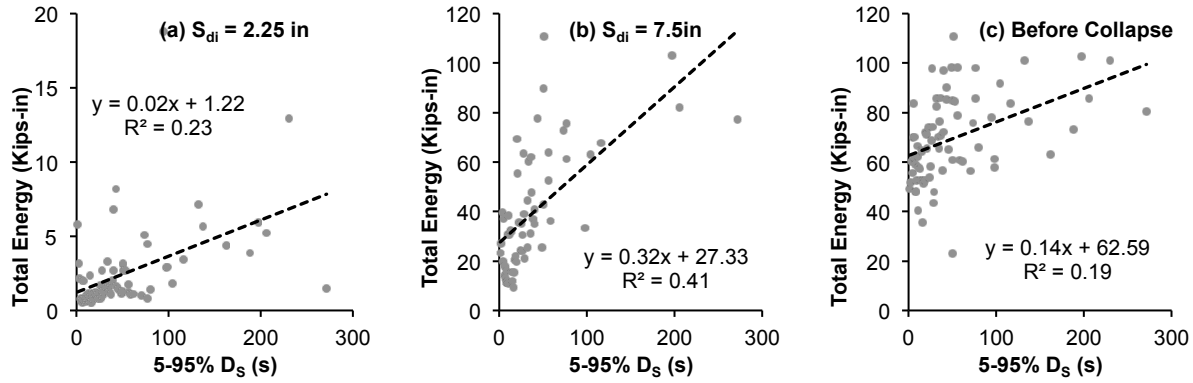


Fig. 10 Total hysteretic energy dissipated by the modern 4-story building (04MP) at ground motion intensity levels of (a) $S_{di} = 2.25$ in, (b) $S_{di} = 7.5$ in and (c) just before collapse.

6.3.3 Effect of Building Properties: Sensitivity Analysis

To further explore the relationship between duration, structural response and building properties, a simplified single-degree-of-freedom (SDOF) model is created and a sensitivity analysis is carried out by varying the SDOF's properties. The nonlinear properties of the SDOF were calibrated such that the static pushover analysis results from the multiple-degree-of-freedom (MDOF) model of the 4-story modern building (04MP) and the SDOF model matched as closely as possible. The SDOF model so calibrated has the same fundamental period, base shear coefficient and ductility capacity as the MDOF, as shown in Fig. 11a. To ensure the SDOF model has similar dynamic and cyclic behavior to the MDOF model, incremental dynamic analysis is carried out on SDOF models with this same backbone, but varying values of the cyclic deterioration parameter, λ . The SDOF model with λ that results in median collapse capacities nearly identical to the MDOF model for groups of short ($0 < 5-95\% D_s < 35s$) and long duration ($5-95\% D_s > 35s$) records is selected as the final calibrated SDOF model, also referred to as the "Base" model.

For the sensitivity analysis, three sets of SDOF models are created from the "Base" model by varying one structural property at a time. The first set of models, referred to as "Set λ ," have the same monotonic pushover backbones, but different energy dissipation capacities, quantified by the model parameter λ . The "Base" model has $\lambda = 35$, and the other SDOF models have lower ($\lambda = 5$ or 20) and higher ($\lambda = 50$ or 65) values, indicating less and more energy dissipation capacity. For comparison, the equivalent SDOF to the ductile 4-story building has $\lambda = 35$ and the equivalent SDOF to the non-ductile 4-story building has $\lambda = 11$. The second set of models, "Set μ ," have different building ductility capacities, but the same fundamental period, base shear, yield displacement, and cyclic deterioration parameters as the "Base" model (Fig. 11b). The "Base" model has a relatively high ductility capacity of 14.8 because it represents a modern, ductile building; the other models comprising Set μ have lower ductility capacities of 3, 8 and 10. The third set of models have different levels of gravity loads applied to the "Base" model, resulting in different levels of P- Δ effects on the structure. This set, referred to as "Set P Δ " and illustrated in Fig. 11c, has the "Base" model with gravity load of 4812 kips applied to the oscillator, the same as the MDOF, and models variations with gravity loads of 1000, 3000, 6000 and 7500 kips.

The SDOF building models are analyzed through IDA with the same set of ground motions used for the MDOF analysis. The analysis results enable us to assess the interaction between ground motion duration and structural response for buildings with different properties. A GLM model using the inverse link function is fitted to results for each SDOF building, to predict the collapse S_{di} as a function of the 5-95% D_s ; the fitted models for each set are illustrated in Fig 12.

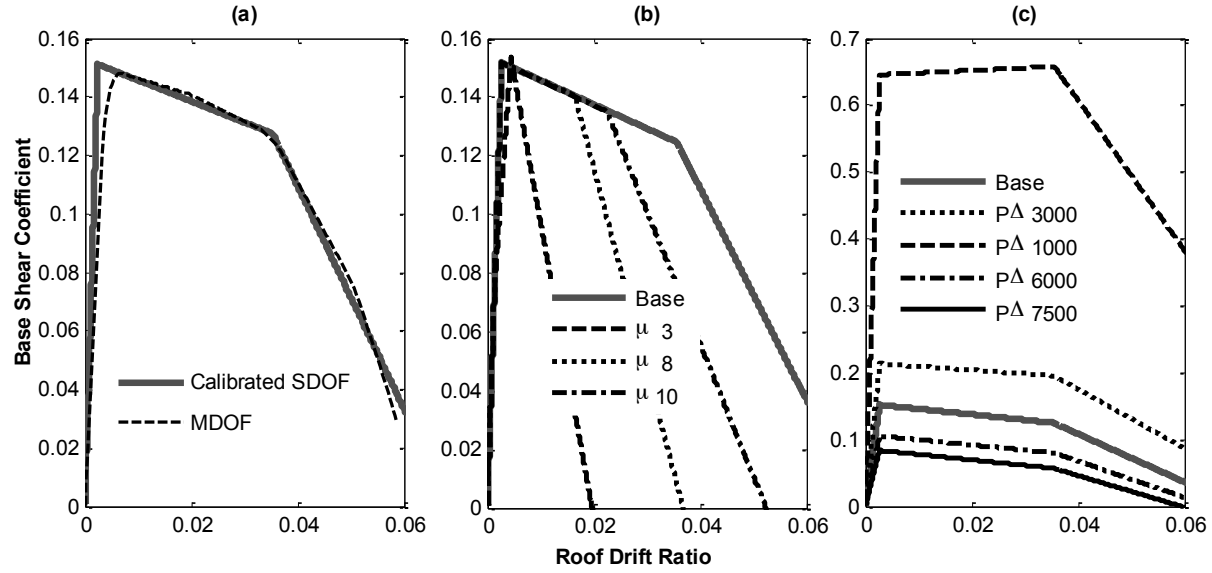


Fig. 11 Pushover results (a) Comparing SDOF “Base” model and MDOF, (b) For SDOF “Set μ ”, (c) For SDOF “Set $P\Delta$ ”

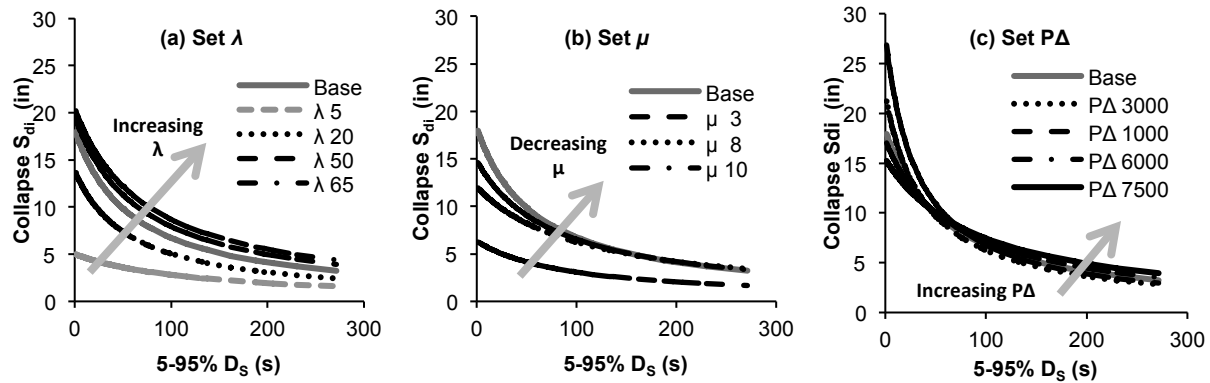


Fig. 12 GLM model fitted for the SDOF models in sensitivity analysis showing effect of duration on response of SDOFs with varying (a) Energy dissipation capacities, (b) Ductility capacities and (c) $P\Delta$ effects.

As expected, decreased energy dissipation capacity, *i.e.* decreased λ , generally brings down the collapse capacity of the structure for all ground motion durations, as shown in Fig. 12a. In addition, the rate of decrease in collapse capacity with duration is bigger for models with more energy dissipation capacity, as indicated by the steeper slopes of the fitted GLM model for greater λ . Similarly for ductility capacity, Fig. 12b shows that the SDOF models with higher ductility capacity have larger collapse capacities, but that the rate of decrease of collapse capacity with duration is higher for more ductile models as compared to the less ductile models. For buildings in “Set $P\Delta$ ”, plotted in Fig. 12c, higher gravity loads cause decrease in overall collapse capacities for shorter durations due to $P\Delta$ deformations, but the collapse capacities become very close in the long duration ground motion range.

These results indicate that duration is having a more significant influence on the collapse capacity of more ductile structures than those that are less ductile, which may seem counter intuitive. All buildings show a decrease in collapse capacity with increasing duration because, as the duration increases, the structure becomes unable to dissipate the energy imposed by so many cycles. Since the weaker, less ductile buildings (*i.e.* low μ_T and low λ) have less overall energy dissipation capacity, even relatively short

duration records may have enough cycles to exhaust their energy dissipation capacity. In contrast, the highly ductile and stronger modern buildings can withstand greater ground motion intensities before collapse for shorter duration earthquakes, but as the duration increases, their capacity to withstand higher intensity ground motions become lesser and lesser because a larger and larger part of their energy dissipation capacity is being utilized. In contrast, past researchers have suggested that duration has a larger influence on more deteriorating systems [43,45]; this is likely because at moderate intensity levels the non-ductile systems will show the effects of duration while the ductile systems will not because the ground motion intensities are not near the collapse capacity of the buildings. Bommer *et al.* [46] found that strength degradation became important at lower ground motion intensity levels under longer duration motions. Although Mahin [47] found P- Δ to be important in an SDOF study, the level of P- Δ does not appear to as significantly influence the duration relationship, as do the cyclic deterioration and ductility capacity parameters. In particular, we note that, for longer duration ground motions, for which the ground motion intensities and displacement demands are less, there is no difference in how duration affects collapse resistance, suggesting that P- Δ does not have a critical impact on collapse in this range.

7. Does Duration Matter for Collapse Risk?

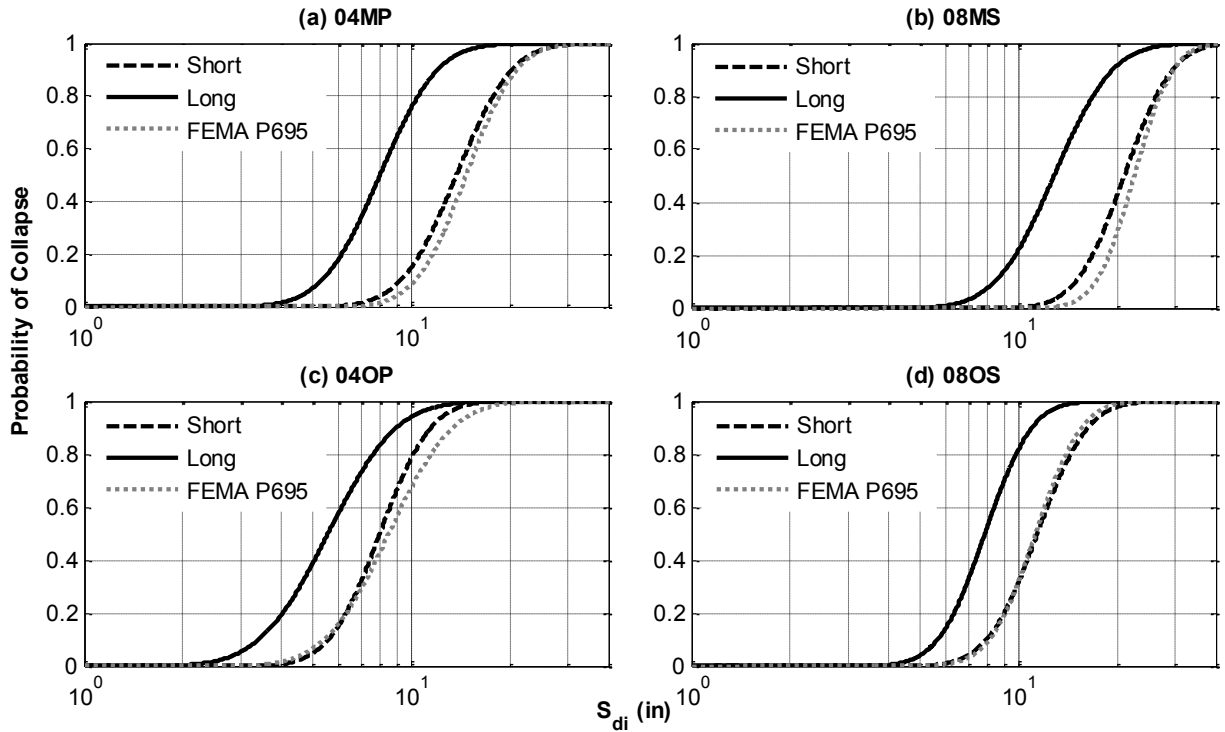


Fig. 13 Collapse fragility functions for *Short* duration, *Long* duration and FEMA P695 [29] far field records for (a) Modern 4-Story building, (b) Modern 8-Story Building, (c) Older 4-Story Building, and (d) Older 8-Story Building.

It can be concluded from the previous sections that ground motion duration influences the structural collapse capacity. To quantify how important this effect is for collapse risk assessment, collapse fragility functions are created for all of the reinforced concrete building models, and four are plotted in Fig. 13. These fragility functions describe the probability of collapse as a function of the ground motion intensity (S_{d1}), assuming a lognormal probability distribution¹. For simplicity of illustration, the ground motion

¹ The Chi-square goodness-of-fit test conducted at the 5% significance level indicates that the lognormal distribution assumption is acceptable for the collapse fragility functions developed for all the buildings. The test indicated lack

records are divided into two groups: *Short* duration records (5-95% D_s : 0-35 s, Median $D_s = 13$ s) and *Long* duration records (5-95% $D_s > 35$ s, Median $D_s = 74$ s), such that there are 39 and 37 records, respectively, in each group. For comparison, these fragility curves are compared to a typical “duration-blind” fragility curve, obtained using the general set of ground motions from FEMA P695 [29]. The fragility curve parameters for all buildings subjected to the *Short* and *Long* and FEMA P695 [29] ground motions are provided in Table 3. The median collapse capacity (denoted x_M in Table 3) quantifies the S_{di} level at which the probability of collapse is 0.50 for each building model.

For the same building, the collapse fragility curve for the *Long* records is consistently located to the left of the collapse fragility curve of *Short* duration records, indicating the increased structural fragility when buildings are subjected to longer duration ground motions. Considering results from all 17 buildings, the *Long* duration records lead to median collapse capacities that are 26 to 56% lower than *Short* duration records. The increase in predicted probability for a given ground motion level may be even more significant; for example, in Fig. 13a, at $S_{di} = 9$ in the probability of collapse predicted by the *Short* duration fragility is 8% compared to 64% predicted by the *Long* duration fragility. The biggest decrease in collapse capacity between the *Short* and *Long* duration records is seen in the modern buildings; similar results were observed in the SDOF sensitivity analysis. In addition, the lognormal standard deviation of the fragility curve (denoted β) which quantifies the dispersion in the prediction, is greater for the *Long* duration fragility curve for most of the buildings, due to the larger variation in the record durations in the *Long* duration set (ranging from 35 to 271.3 s). As can be seen in Fig. 13, the FEMA P695 [29] ground motions predict collapse fragilities very similar to those obtained using the *Short* duration ground motions (on average approximately a 5% difference in median collapse capacities).

The results show clearly that the longer duration records make a structure more fragile, and current risk assessment methodologies, which evaluate the collapse capacity of structure without consideration of ground motion duration, may not give a clear picture of collapse risk at sites that are more likely to experience long duration ground motions. A comprehensive risk assessment, which accounts for the probability distribution of different duration ground motions occurring at a particular site, is outside the scope of this study. Nonetheless, to explore the effects of duration on risk, we note that a number of researchers have proposed empirical predictions for duration of ground motion at a site, as a function of earthquake magnitude, site-to-source distance, and other parameters [14,48,49], and apply these relationships to compare predicted durations at a Seattle site and a San Francisco site. The earthquake scenarios contributing most to the hazard of having a 2% in 50 year ground motion event at a rock site in Seattle and San Francisco are obtained from seismic deaggregation of probabilistic seismic hazard analysis by USGS [1]. The deaggregation generated the most important earthquake scenarios for the selected hazard level as a M_w 7.74 earthquake with closest distance ($R_{closest}$) of 12.5 km for the San Francisco site and a M_w 9.02 earthquake with $R_{closest} = 109$ km for the Seattle site. Using the relationship proposed by Abrahamson and Silva [48], the expected ground motion durations from these earthquakes are about 27s and 95s for the San Francisco and Seattle rock sites, respectively. For a ductile concrete building having a period of 1s, this difference in ground shaking durations corresponds to 40% reduction in median collapse resistance.

This illustrative calculation of collapse risk in Seattle and San Francisco is based on one of the important earthquake scenarios only at each site and examines the effect of duration, all else being equal. In a complete probabilistic seismic hazard analysis of the collapse risk of a particular building at a particular site, it is necessary to consider all of the possible earthquake scenarios which could affect a site, as well as the distribution of ground motion intensities and durations associated with those events. To do so, more

of fit for a few of the buildings’ *Long* duration fragility curves, due to the wide variability of response predictions associated with records with very different duration. Since the test indicated acceptability of the lognormal assumption for more than 75% of the buildings subjected to the long duration set, the assumption is taken as valid.

data are needed to improve the ground motion duration prediction equations. Since the existing relationships have been mostly developed using a limited ground motion database consisting of shallow crustal events with moderate magnitudes and distances up to 200 km, they may not be suitable for predicting expected duration for subduction earthquakes and other larger magnitude events (especially those dominating the hazard in Seattle). In addition, most ground motion prediction equations for intensity predict $S_a(T_1)$ not S_{di} , although, in future, more attenuation relationship for S_{di} may be developed (e.g. [38]). A better understanding of the probability distribution of ground motion intensities and durations at a site, combined with the fragility curves in Fig. 13, is needed to obtain robust estimates of the collapse risk of structures at a site due to possible occurrence of a long or short duration ground motions.

Table 3 Summary of collapse fragility function parameters for all buildings subjected to *Short, Long* and FEMA P695 [29] ground motions

ID	Short 5-95 % D_s		Long 5-95% D_s		FEMA P695		Variation in Median Capacities Compared to x_{ms}	
	x_{ms} (in)	β_s	x_{mL} (in)	β_L	x_{mF} (in)	β_F	x_{mI}	x_{mF}
02MS	11	0.36	5.9	0.48	13	0.32	-48%	16%
04MP	14	0.31	8.0	0.32	15	0.28	-42%	7%
04MS	14	0.40	6.2	0.40	15	0.33	-56%	8%
08MP	16	0.28	11	0.34	17	0.23	-33%	8%
08MS	21	0.27	13	0.32	23	0.21	-39%	7%
12MP	20	0.33	14	0.34	22	0.28	-33%	9%
12MS	22	0.30	14	0.32	24	0.25	-34%	10%
20MP	28	0.26	20	0.30	32	0.25	-30%	15%
20MS	31	0.31	19	0.34	34	0.33	-38%	11%
02OS	5.0	0.21	3.3	0.30	5.0	0.21	-33%	1%
02OP	6.4	0.31	3.6	0.28	6.6	0.26	-43%	4%
04OP	8.0	0.28	5.6	0.38	8.5	0.35	-31%	6%
04OS	10	0.28	6.8	0.23	10	0.21	-30%	0%
08OP	9	0.27	6.5	0.31	9.1	0.34	-26%	3%
08OS	11	0.28	7.9	0.26	11	0.25	-31%	-1%
12OP	13	0.45	8.7	0.27	11	0.33	-31%	-17%
12OS	13	0.27	9.2	0.25	12	0.23	-30%	-5%

8. Conclusions

Based on the results described above, we conclude that ground motion duration plays a significant role in the collapse resistance of a structure. The consistent trend observed across all the buildings is that the collapse capacity of a particular structure, quantified by the ground motion intensity at which collapse occurs, decreases as the duration of the record increases. As a consequence, when we consider two ground motions with the same intensity, the longer duration record proves more damaging for the structure than shorter duration record because the longer duration ground motion imposes higher energy demands on the structure. Even so, duration does not have much influence on the maximum drift responses of the structure. These results suggest that a vector of ground motion parameters that reflect ground motion intensity, frequency content and duration can provide better predictions of earthquake-induced collapse than an assessment that neglects duration; in this study, the ground motion intensity parameter S_{di} represented both intensity and frequency content. The significance of ground motion duration for collapse capacity depends on the ductility capacity and energy dissipation characteristics of the structure, as well as the intensity of ground motions expected at a particular site.

Current methods of building design and assessment do not typically consider the effect of ground motion duration. The vast majority of buildings are designed according to static methods based on a code-defined design spectrum. In rare cases, nonlinear time history analyses are used in design, but it is not required by most codes to consider duration of records in ground motion selection procedures. However, these results indicate that longer duration ground motions make a structure more fragile and therefore, if we apply “duration blind” analyses at sites where long duration ground motions can be expected, we may be underestimating the risk of collapse of the structure.

The influence of duration on structural collapse informs the procedure generally adopted to select ground motions for nonlinear analysis of structures. Matching response spectra of the selected ground motions with the target design spectra or conditional mean spectra explicitly accounts for the intensity and frequency content of expected ground motions, but not duration. The ground motion duration is implicitly considered by matching parameters like magnitude, distance to site etc. for selected ground motions with hazard deaggregation, but it does not guarantee that the influence of expected duration on structural will be completely captured with the ground motion set so selected. Thus, our findings support recommendations by [50–52] justifying ground motion duration as one of the parameters to consider in ground motion selection.

More research is needed before comprehensive risk assessments can be conducted that accounts for ground motion duration in the framework of performance-based earthquake engineering. First, probabilistic seismic hazard analyses that represent the joint probability of occurrence of ground motion intensity and duration at a particular site are needed. Longer duration ground motions tend to be less intense, but this depends on the site seismicity; duration is positively correlated with site-to-source distance and earthquake magnitude, but ground motion intensity is inversely correlated with distance. This effort is complicated by the wide variation in ground motion duration predictions, even for a given set of earthquake properties, and by differences in ground motion frequency content between long and short duration ground motions. More investigation of the relationship between the earthquake source (*i.e.* interface vs. intraslab vs. crustal) and duration prediction is also needed. In addition, although this study examined a wide number of buildings with varying properties, different types of structures with different approaches to modeling cyclic deterioration and different failure mechanisms (*e.g.* shear critical columns) should also be examined to verify that results can be further extrapolated to other types of structures.

9. Acknowledgments

The authors would also like to thank Nicolas Luco, Rajagopalan Balaji, Keith Porter and two anonymous reviewers for their input to the study and findings.

10. References

- [1] United States Geological Survey < <http://www.usgs.gov/> > ; 2012.
- [2] Luca FD, Chioccarelli E, Iervolino I. Preliminary study of the 2011 Japan earthquake ground motion record V1.01. 2011, available at <<http://www.reluis.it>>.
- [3] Pacific Earthquake Engineering Research Center (PEER). PEER NGA Database < <http://peer.berkeley.edu/nga/> >; 2011.
- [4] ASCE. Minimum design loads for buildings and other structures (7-10). 2010.
- [5] Bray J. Simplified seismic slope displacement procedures. *Earthquake Geotechnical Engineering*, 2007, pp. 327–53.
- [6] Green RA, Terri GA. Number of equivalent cycles concept for liquefaction evaluations—revisited. *Journal of Geotechnical and Geoenvironmental Engineering* 2005;131:477.
- [7] Hancock J, Bommer JJ. A state-of-knowledge review of the influence of strong-motion duration on structural damage. *Earthquake Spectra* 2006;22:827.

- [8] Baker JW, Allin Cornell C. A vector-valued ground motion intensity measure consisting of spectral acceleration and epsilon. *Earthquake Engineering & Structural Dynamics* 2005;34:1193–217.
- [9] Ibarra LF, Medina RA, Krawinkler H. Hysteretic models that incorporate strength and stiffness deterioration. *Earthquake Engineering & Structural Dynamics* 2005;34:1489–511.
- [10] Zareian F, Krawinkler H. Assessment of probability of collapse and design for collapse safety. *Earthquake Engineering & Structural Dynamics* 2007;36:1901–14.
- [11] Haselton CB, Liel AB, Deierlein GG, Dean BS, Chou JH. Seismic Collapse Safety of Reinforced Concrete Buildings. I: Assessment of Ductile Moment Frames. *Journal of Structural Engineering* 2011;137:481.
- [12] Ruiz-Garcia J. On the influence of strong-ground motion duration on residual displacement demands. *Earthquake and Structures* 2010;1:327–44.
- [13] Iervolino I, Manfredi G, Cosenza E. Ground motion duration effects on nonlinear seismic response. *Earthquake Engineering & Structural Dynamics* 2006;35:21–38.
- [14] Bommer JJ, Stafford PJ, Alarcón JE. Empirical equations for the prediction of the significant, bracketed, and uniform duration of earthquake ground motion. *Bulletin of the Seismological Society of America* 2009;99:3217–33.
- [15] Bommer JJ, Martínez-Pereira A. The effective duration of earthquake strong motion. *Journal of Earthquake Engineering* 1999;3:127–72.
- [16] Trifunac MD, Brady AG. A study on the duration of strong earthquake ground motion. *Bulletin of the Seismological Society of America* 1975;65:581.
- [17] Foschaar JC, Baker JW, Deierlein GG. Preliminary Assessment of Ground Motion Duration Effects on Structural Collapse. *Proceedings of the 15th World Conference on Earthquake Engineering*, 2012.
- [18] COSMOS. COSMOS Virtual Data Center < <http://db.cosmos-eq.org/> > ; 2011.
- [19] United States Geological Survey. National Strong-Motion Project < <http://nsmp.wr.usgs.gov/> > ; 2012.
- [20] Yang J. Nonlinear responses of high-rise buildings in giant subduction earthquakes. Ph.D Thesis. California Institute of Technology, 2009.
- [21] Baker JW. Quantitative classification of near-fault ground motions using wavelet analysis. *Bulletin of the Seismological Society of America* 2007;97:1486.
- [22] Kramer SL. *Geotechnical earthquake engineering*. Prentice Hall; 1996.
- [23] Atkinson GM, Boore DM. Empirical ground-motion relations for subduction-zone earthquakes and their application to Cascadia and other regions. *Bulletin of the Seismological Society of America* 2003;93:1703–29.
- [24] Liel AB, Haselton CB, Deierlein GG. Seismic collapse safety of reinforced concrete buildings. II: comparative assessment of nonductile and ductile moment frames. *Journal of Structural Engineering* 2011;137:492.
- [25] ICC. *International building code 2003*. International Code Council; 2003.
- [26] ASCE. *Minimum design loads for buildings and other structures (7-05)*. 2005.
- [27] ACI. *Building code requirements for structural concrete (ACI 318-02)*. American Concrete Institute; 2002.
- [28] ICBO. *Uniform building code*. 1967.
- [29] FEMA. *Quantification of building seismic performance factors FEMA P695* 2009.
- [30] OpenSees. *Open System for Earthquake Engineering Simulation* < <http://opensees.berkeley.edu/> > ; 2012.
- [31] Haselton CB, Liel AB, Lange ST, Deierlein GG. PEER Report 2007/03 Beam-column element model calibrated for predicting flexural response leading to global collapse of RC frame buildings. 2008.
- [32] Elwood KJ. Modelling failures in existing reinforced concrete columns. *Canadian Journal of Civil Engineering* 2004;31:846–59.
- [33] Ghannoum WM, Moehle JP, Bozorgnia Y. Analytical collapse study of lightly confined reinforced concrete frames subjected to northridge earthquake ground motions. *Journal of Earthquake Engineering* 2008;12:1105–19.
- [34] Vamvatsikos D, Cornell CA. Incremental dynamic analysis. *Earthquake Engineering & Structural Dynamics* 2002;31:491–514.

- [35] Baker JW, Allin Cornell C. Spectral shape, epsilon and record selection. *Earthquake Engineering & Structural Dynamics* 2006;35:1077–95.
- [36] Matsumura K. On the intensity measure of strong motions related to structural failures. *Proceedings of the 10th World Conference on Earthquake Engineering*, vol. 1, 1992, pp. 375–80.
- [37] Tothong P, Luco N. Probabilistic seismic demand analysis using advanced ground motion intensity measures. *Earthquake Engineering & Structural Dynamics* 2007;36:1837–60.
- [38] Tothong P, Cornell CA. An empirical ground-motion attenuation relation for inelastic spectral displacement. *Bulletin of the Seismological Society of America* 2006;96:2146–64.
- [39] Fox J. *Applied regression analysis and generalized linear models*. SAGE; 2008.
- [40] Myers RH, Montgomery DC, Vining GG, Robinson TJ. *Generalized linear models: with applications in engineering and the sciences*. John Wiley & Sons; 2010.
- [41] R. The R project for statistical computing < <http://www.r-project.org/> > ; 2011.
- [42] Weisberg S. *Applied linear regression*. John Wiley & Sons; 2005.
- [43] Elnashai A, Sarno LD. *Fundamentals of earthquake engineering*. 1st ed. Wiley; 2008.
- [44] Champion C, Liel A. The effect of near-fault directivity on building seismic collapse risk. *Earthquake Engineering & Structural Dynamics* 2012;n/a–n/a.
- [45] Amadio C, Fragiaco M, Rajgelj S. The effects of repeated earthquake ground motions on the non-linear response of SDOF systems. *Earthquake Engineering & Structural Dynamics* 2003;32:291–308.
- [46] Bommer J, Magenes G, Hancock J, Penazzo P. The influence of strong-motion duration on the seismic response of masonry structures. *Bulletin of Earthquake Engineering* 2004;2:1–26.
- [47] Mahin SA. Effects of duration and aftershocks on inelastic design earthquakes. *Proceedings of the Seventh World Conference on Earthquake Engineering*, Istanbul, vol. 5, 1980, pp. 677–80.
- [48] Abrahamson NA, Silva WJ. *Empirical ground motion models*. Report to Brookhaven National Laboratory 1996.
- [49] Kempton JJ, Stewart JP. Prediction equations for significant duration of earthquake ground motions considering site and near-source effects. *Earthquake Spectra* 2006;22:985.
- [50] Bradley BA. Correlation of significant duration with amplitude and cumulative intensity measures and its use in ground motion selection. *Journal of Earthquake Engineering* 2011;15:809–32.
- [51] Katsanos EI, Sextos AG, Manolis GD. Selection of earthquake ground motion records: A state-of-the-art review from a structural engineering perspective. *Soil Dynamics and Earthquake Engineering* 2010;30:157–69.
- [52] Malhotra PK. Strong-motion records for site-specific analysis. *Earthquake Spectra* 2003;19:557.
- [53] Caltech. Caltech Virtual Shaker <<https://virtualshaker.caltech.edu/>>; 2011.

Appendix A: Ground Motion Database

Table A.1 Ground motion database

Year	Earthquake	$M^{[e]}/(M_w)$	Epi. Dis.(km)	Type	Station or ID	Soil ^[g]	PGA (g)	5-95% D_s (s)
1980 ^[a]	Mammoth Lakes	4.8	1.1	Crustal	NGA0264	D	0.53	1.1
1935 ^[a]	Helena, Montana	6	6.3	Crustal	NGA0001	C	0.15	2.3
1980 ^[a]	Mammoth Lakes	5.7	2.8	Crustal	NGA0240	D	0.43	3.5
1976 ^[a]	Friuli, Italy	6.5	20.2	Crustal	NGA0125	C	0.35	4.2
1976 ^[a]	Friuli, Italy	6.5	20.2	Crustal	NGA0125	C	0.30	4.9
1994 ^[a]	Northridge	6.7	26.5	Crustal	NGA0960	D	0.48	5.6
1989 ^[a]	Loma Prieta	6.9	31.4	Crustal	NGA0767	D	0.54	6.4
1989 ^[a]	Loma Prieta	6.9	94	Crustal	NGA0783	D	0.27	7
1994 ^[a]	Northridge	6.7	16.3	Crustal	NGA0952	C	0.39	7.6
1992 ^[a]	Landers	7.3	82.1	Crustal	NGA0848	D	0.31	8.2
1999 ^[a]	Duzce, Turkey	7.1	41.3	Crustal	NGA1602	D	0.73	8.5
1994 ^[a]	Northridge	6.7	13.4	Crustal	NGA0953	D	0.42	9.2
1979 ^[a]	Imperial Valley	6.5	12.4	Crustal	NGA0189	D	0.29	10
1999 ^[a]	Kocaeli, Turkey	7.5	98.2	Crustal	NGA1158	D	0.33	10.6
1979 ^[a]	Imperial Valley	6.5	17.7	Crustal	NGA0162	D	0.27	11
1994 ^[a]	Northridge	6.7	25.5	Crustal	NGA1003	D	0.47	11.5
1995 ^[a]	Kobe, Japan	6.9	24.2	Crustal	NGA1107	D	0.34	12.9
1987 ^[a]	Superstition Hills	6.5	11.2	Crustal	NGA0725	D	0.45	13.8
1979 ^[a]	Imperial Valley	6.5	17.6	Crustal	NGA0162	D	0.17	14.6
1992 ^[a]	Cape Mendocino	7	22.6	Crustal	NGA0829	D	0.24	15.3
1987 ^[a]	Superstition Hills	6.5	35.8	Crustal	NGA0721	D	0.36	16
1989 ^[a]	Loma Prieta	6.9	48.2	Crustal	NGA0776	C	0.37	16.4
1989 ^[a]	Loma Prieta	6.9	47.9	Crustal	NGA0777	D	0.25	17.4
1992 ^[a]	Landers	7.3	86	Crustal	NGA0900	D	0.15	18.9
1987 ^[a]	Superstition Hills	6.5	19.5	Crustal	NGA0728	D	0.16	19.6
1986 ^[a]	Taiwan SMART	7.3	77.6	Subduction	NGA0578	D	0.24	20.3
1986 ^[a]	Hollister	5.4	14.8	Crustal	NGA0498	D	0.10	21.2
1985 ^[b]	Valparaiso	7.8	85.7	Subduction	Melipilla	A/B	0.53	22.4
1999 ^[a]	Chi-Chi, Taiwan	7.6	40.5	Crustal	NGA1182	C	0.30	24.3
1990 ^[a]	Manjil, Iran	7.4	84	Crustal	NGA1636	D	0.13	25.7
1992 ^[a]	Landers	7.3	13.7	Crustal	NGA0864	C	0.28	26.1
1992 ^[a]	Landers	7.3	13.7	Crustal	NGA0864	C	0.27	27.2
1999 ^[a]	Hector Mine	7.1	48	Crustal	NGA1762	D	0.18	27.5
1999 ^[a]	Chi-Chi, Taiwan	7.6	32	Crustal	NGA1595	D	0.33	28.3
1990 ^[a]	Manjil, Iran	7.3	40.4	Crustal	NGA1633	C	0.51	28.9
1992 ^[a]	Landers	7.3	27.3	Crustal	NGA0850	D	0.17	31.8
1992 ^[a]	Landers	7.3	21.3	Crustal	NGA0881	D	0.13	32.1
1985 ^[b]	Valparaiso	7.8	115	Subduction	San Felipe, Chile	D/E	0.43	33.7
1999 ^[a]	Chi-Chi, Taiwan	7.6	28.4	Crustal	NGA1536	D	0.18	34.6
1979 ^[a]	St Elias, Alaska	7.5	74.8	Crustal	NGA1628	D	0.09	35.5
1992 ^[a]	Landers	7.3	32.3	Crustal	NGA0882	D	0.11	36.3
1992 ^[a]	Landers	7.3	32.3	Crustal	NGA0882	D	0.10	37

Year	Earthquake	M ^[e] (M _w)	Epi. Dis.(km)	Type	Station or ID	Soil ^[g]	PGA (g)	5-95% D _s (s)
1999 ^[a]	Chi-Chi, Taiwan	7.6	33.8	Crustal	NGA1547	D	0.12	38.7
2002 ^[a]	CA/Baja Border	5.3	42.2	Crustal	NGA2003	D	0.04	39.9
1985 ^[b]	Valparaiso	7.8	74.3	Subduction	Zapallar	A/B	0.31	40.4
1985 ^[b]	Valparaiso	7.8	~ 65	Subduction	San Isidro	^[f]	0.68	42.6
2002 ^[a]	CA/Baja Border	5.3	42.2	Crustal	NGA2003	D	0.08	43.6
1999 ^[a]	Chi-Chi, Taiwan	7.6	41.4	Crustal	NGA1246	D	0.19	45.9
1985 ^[b]	Valparaiso	7.8	25.4	Subduction	el Almendral	^[f]	0.30	48.4
1985 ^[b]	Valparaiso	7.8	25.4	Subduction	el Almendral	^[f]	0.16	49.9
2007 ^[c]	KM, Indonesia	7.9	164.6	Subduction	West Sumatra	^[f]	0.13	50.3
1979 ^[a]	Imperial Valley	6.5	33.7	Crustal	NGA0169	D	0.35	50.3
1979 ^[a]	Imperial Valley	6.5	33.7	Crustal	NGA0169	D	0.22	51
2007 ^[c]	KM, Indonesia	7.9	164.6	Subduction	West Sumatra	^[f]	0.09	52.9
1985 ^[b]	Valparaiso	7.9	25.3	Subduction	Ventanas	^[f]	0.20	55.9
1985 ^[b]	Valparaiso	7.9	25.3	Subduction	Ventanas	^[f]	0.23	56.3
1995 ^[a]	Kobe,Japan	6.9	47.5	Crustal	NGA1113	D	0.08	58.3
1999 ^[a]	Chi-Chi, Taiwan	7.6	69.3	Crustal	NGA1183	D	0.12	61.4
1995 ^[a]	Kobe,Japan	6.9	47.5	Crustal	NGA1113	D	0.06	70.6
2002 ^[a]	Denali, Alaska	7.9	189.6	Crustal	NGA2115	C	0.08	73.6
2002 ^[a]	Denali, Alaska	7.9	189.6	Crustal	NGA2115	C	0.07	76.6
1999 ^[a]	Chi-Chi, Taiwan	7.6	71.6	Crustal	NGA1181	D	0.10	76.9
1999 ^[a]	Chi-Chi, Taiwan	7.6	71.6	Crustal	NGA1181	D	0.10	80.1
2002 ^[a]	Denali, Alaska	7.9	148.1	Crustal	NGA2109	D	0.04	94.4
2002 ^[a]	Denali, Alaska	7.9	93.4	Crustal	NGA2113	C	0.07	97.4
2002 ^[a]	Denali, Alaska	7.9	93.4	Crustal	NGA2113	C	0.06	98.7
2002 ^[a]	Denali, Alaska	7.9	150	Crustal	NGA2110	C	0.07	104.2
2002 ^[a]	Denali, Alaska	7.9	296.4	Crustal	NGA2104	D	0.02	116.1
n/a ^[d]	Cascadia	9.2	446.8	Subduction	Seattle	B/C	0.16	132.3
n/a ^[d]	Cascadia	9.2	446.8	Subduction	Seattle	B/C	0.13	137.2
n/a ^[d]	Cascadia	9.2	481.3	Subduction	Seattle	B/C	0.05	162.2
n/a ^[d]	Cascadia	9.2	481.3	Subduction	Seattle	D/E	0.13	188
n/a ^[d]	Cascadia	9.2	446.8	Subduction	Seattle	D/E	0.16	196.7
n/a ^[d]	Cascadia	9.2	481.3	Subduction	Seattle	D/E	0.14	206
n/a ^[d]	Cascadia	9.2	446.8	Subduction	Seattle	D/E	0.18	230.1
n/a ^[d]	Cascadia	9.2	481.3	Subduction	Seattle	B/C	0.04	271.3

^[a] Database: PEER Next Generation Attenuation (NGA) database [3]

^[b] Database: COSMOS Virtual Data Center [18]

^[c] Database: USGS National Strong-Motion Project [19]

^[d] Database: Simulated Ground Motions - Caltech Virtual Shaker [20,53]

^[e] Earthquake Magnitude

^[f] Data not available

^[g] NEHRP Soil Classification [4]

Part 2: Collapse Risk of Buildings in the Pacific Northwest Region due to Subduction Earthquakes

1. Motivation

Recent seismic events in Sumatra, Indonesia (M_w 9.1, 2004), Tohoku, Japan (M_w 9.0, 2011), and Maule, Chile (M_w 8.8, 2010) are some of the largest earthquakes ever recorded (USGS 2012a). These subduction earthquakes occur when an oceanic tectonic plate subducts beneath a continental plate and there is a rupture (a) at the interface of the two plates (*interface* events) or (b) deep within the subducting plate (*intraslab* events). In the Cascadia subduction zone in the Pacific Northwest region of the U.S. and Canada, the Juan de Fuca, Explorer and Gorda Plates are subducting beneath the North American Plate (Figure 14(a)).

In the last 3500 years, at least seven large subduction earthquakes ($M_w > 9$) have occurred in the Cascadia subduction zone; the latest one occurred in January, 1700. These events have an estimated return period of 400 to 600 years (Pacific Northwest Seismic Network 2012; USGS 2012a). On this basis, seismologists expect a similar subduction earthquake to occur in the future that could potentially endanger life, structures and infrastructure in Portland, Oregon (metro area population ~2.3 million), Seattle, Washington (3.9 million), Vancouver, British Columbia (2.3 million) and other communities in this region (Government of Canada 2012; US Census 2012). Indeed, Mahsuli and Haukaas (2013) assessed the seismic risk of Vancouver using first and second-order reliability methods, finding that among different sources of seismicity in the region, earthquakes from subduction sources have the highest probability of producing losses exceeding \$100 billion.

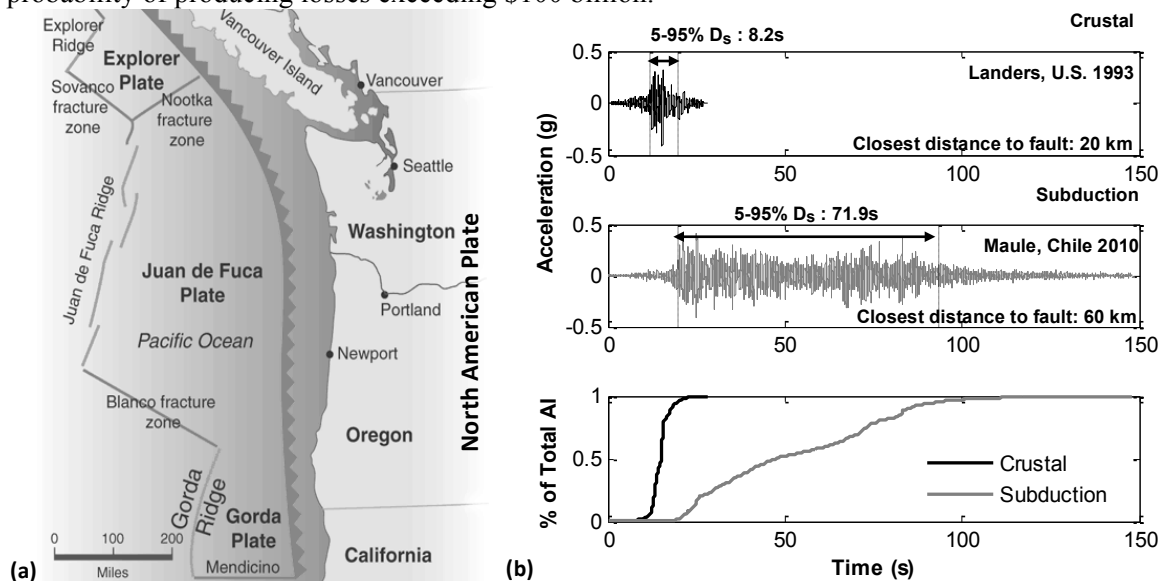


Figure 14. (a) Cascadia subduction zone map (from Thatcher 2001); (b) Ground motion time histories and Arias intensity for crustal and subduction records having the same PGA, but different durations

Ground motions from subduction earthquakes are generally longer in duration as compared to ground motions from more frequently recorded shallow crustal events. Figure 14(b) shows selected ground motion time histories with the same peak ground acceleration (PGA) of 0.42g from crustal and subduction earthquakes. Duration is quantified as the 5-95% significant duration, denoted 5-95% D_s , which is calculated as the time between which 5 to 95% of the energy of the accelerogram (quantified by the Arias Intensity, AI) is accumulated (Bommer and Martínez-Pereira 1999). The subduction ground motion has substantially longer duration than the crustal ground motion because of two factors significantly

influencing duration of ground motion at a site: (1) the higher magnitude of the subduction event; and (2) the greater source-to-site distance (Bommer et al. 2009).

Subduction ground motions may also have different frequency content characteristics from crustal ground motions. Figure 15(a) compares the mean response spectra for crustal and subduction earthquakes ($M_w = 7$, $R = 50\text{km}$, $V_{s30} = 537\text{m/s}$) based on ground motion prediction equations (Abrahamson et al. 2012; Atkinson and Boore 2003; Atkinson and Macias 2009; Zhao 2006). Figure 15(a) illustrates that, for the same magnitude earthquake and source-to-site distance, ground motions from interface and intraslab subduction earthquakes are expected to produce higher intensity shaking than crustal earthquakes at shorter periods; at longer periods this difference diminishes. However, the Cascadia Subduction zone's interface earthquakes are likely to have large magnitude and also large source-to-site distances (Atkinson and Boore 2003). For this reason, Figure 15(a) also compares the expected crustal response spectra for $M_w = 7$ and $R = 50\text{km}$ to the expected interface response spectra for $M_w = 9$ and $R = 200\text{km}$. This comparison shows that subduction attenuation relations predict ground motion intensities similar to crustal ground motion intensities recorded at shorter distances because the subduction interface ground motion intensities attenuate at a slower rate than crustal ground motions with distance from the rupture. In addition, the subduction (interface) spectrum has higher expected intensities at longer periods as compared to the crustal spectra. Figure 15(b) provides a better comparison of the spectral shape, where the response spectra are scaled to the same spectral intensity at 1s, showing the difference in frequency content between the ground motions from large magnitude subduction events and the other cases.

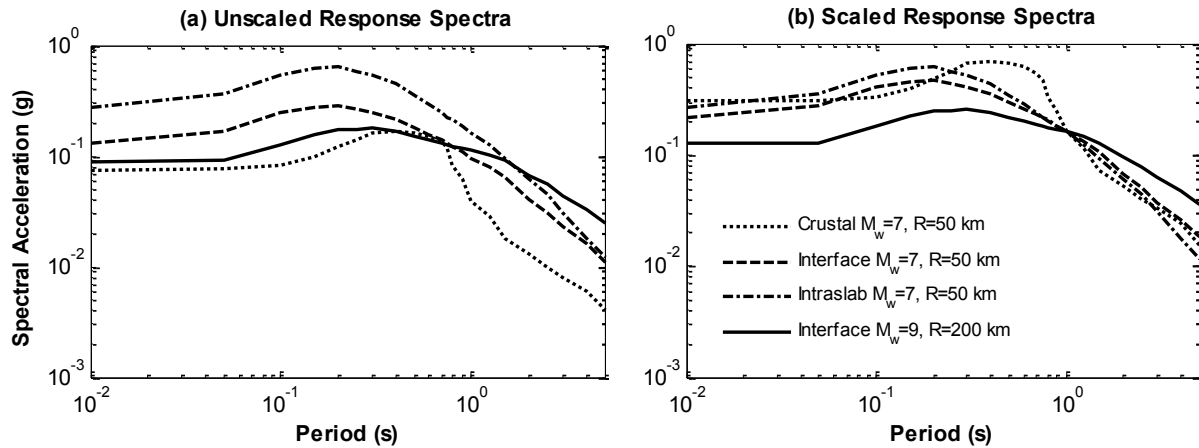


Figure 15. Mean response spectra from ground motion prediction equations for crustal and subduction earthquakes at a site with $V_{s30}=537\text{m/s}$: (a) unscaled and (b) scaled to 1.6g at $T = 1\text{s}$. Multiple ground motion prediction equations are used and weighted as in USGS (2012a) seismic hazard computations.

The duration and frequency content characteristics of large magnitude subduction earthquakes may affect structural response differently than ground motions from crustal earthquakes. In the Michoacan (Mexico City) subduction earthquake (M_w 8.2, 1985), around 20% of the 6 to 15-story buildings located in the region of greatest damage were damaged or collapsed; this damage was attributed to substantial long period spectral content of the ground motions produced by basin amplification effects (Beck and Hall 1986). Yang (2009) examined the susceptibility of structures to subduction ground motions by analyzing 20-story steel moment frames subjected to ground motions from the Tokachi Oki, Japan earthquake (M_w 8.3, 2003). Yang (2009) found that these buildings did not collapse under the as-recorded motions, but collapse would occur if ground motion intensity increased by as little as 6-12.5%. White and Ventura (2004) conducted nonlinear dynamic analyses on a 30-story residential building in Vancouver, Canada comparing the effect of a pair of crustal and subduction ground motions with the same PGA , finding that the structural response was more influenced by higher mode effects and torsional effects in the case of subduction ground motions. Longer ground motion duration has also been shown more generally to

reduce structural collapse capacity (Hancock and Bommer 2006). Raghunandan and Liel (2013) conducted nonlinear dynamic analysis of 17 ductile and non-ductile RC moment frames and found a significant decrease in collapse capacity on being subjected to longer duration ground motions as compared to shorter duration motions. Chandramohan *et al.* (2013) reached a similar conclusion about the effects of ground motion duration on the collapse capacity of steel moment frames. Taken together, these studies indicate that structural response differs for crustal and subduction earthquakes, due to characteristics of subduction ground motion duration and frequency content.

Nevertheless, the influence of the unique characteristics of ground motions from subduction earthquakes on probabilistic metrics of building performance and safety is uncertain. Recent studies (*e.g.* FEMA 2009; Haselton *et al.* 2011; Krishnan and Muto 2008) have quantified the collapse risk of modern code-conforming structures in California subjected to crustal motions. In fact, new risk-targeted seismic design maps in current building codes and standards in the U.S. (ASCE 2010; ICC 2012) define site-specific spectral values for building design that are intended to provide a uniform collapse risk of 1% in 50 years at sites across the U.S. (Luco *et al.* 2007). However, the collapse risk of structures designed according to these codes in the Pacific Northwest remains poorly understood, due to the scarcity of studies quantifying structural performance on exposure to subduction ground motions. It is also not clear how older buildings with known deficiencies, such as non-ductile concrete structures (Liel and Deierlein 2012), will perform under subduction ground shaking.

Buildings in the Pacific Northwest region are potentially at risk of ground shaking from crustal (*e.g.* Seattle fault), and interface and intraslab subduction earthquakes. This paper assesses the risk of earthquake-induced building collapse in the Pacific Northwest, accounting for the unique characteristics of subduction ground motions. For this purpose, 24 RC moment frame buildings are designed according to outdated building codes (1967, 1973, 1994 Uniform Building Code) and modern building codes (2012 International Building Code) for Portland and Seattle. RC moment frames have been a relatively prevalent type of construction in the cities of Portland and Seattle since the 1940s (Don 2007; EERI 2005), making them a suitable choice of structural system for studying the collapse risk of buildings constructed in the region. Nonlinear analytical models that are capable of capturing key failure modes of non-ductile and ductile concrete frames to the point of structural collapse are generated for each of the RC frames. Incremental dynamic analysis is carried out on these building models using two ground motion sets: *Crustal* and *Subduction*. In this study, dynamic simulation results are summarized in the form of collapse fragility curves (representing the probability of collapse conditioned on ground motion intensity) that are calculated for each set of ground motions and compared with each other. These fragility curves are integrated with seismic hazard information for sites in Portland and Seattle to predict the risk of earthquake-induced collapse.

2. Ground Motion Database

In order to quantify the collapse capacities of buildings subjected to crustal and subduction ground motions, a ground motion database is compiled with motions from both types of events. The “*Crustal*” set consists of 35 far-field crustal ground motions selected from the set of 44 ground motions used in FEMA P-695 (FEMA 2009). These records are from large magnitude shallow crustal earthquakes (M_w 6.5-7.6), recorded at moderate distances from the rupture (7-26 km) with $PGA > 0.15g$. The “*Subduction*” set consists of 42 ground motions from primarily interface subduction events (M_w 6.8-9.0), collected from a number of different databases (CESMD 2012; K-NET 2012; NOAA 2012; PEER 2012; USGS 2012b). This set includes recordings from the recent Tohoku, Japan (M_w 9.0, 2011) and Maule, Chile (M_w 8.8, 2010) events, and recordings from subduction earthquakes in Alaska and Washington states, as well as Chile, El Salvador, Indonesia, Japan, and Mexico. These ground motions have $PGA > 0.01g$ (60% having $PGA > 0.15g$) and are recorded at larger distances from the rupture (27-392 km). Although there are 17 low PGA records in the set, for the most part, the *Subduction* ground motions have

relatively large *PGAs* despite being recorded at large distances from the source. The K-NET (2012) Japanese earthquake recordings were baseline corrected (zeroth order) and filtered with a 4th order Butterworth filter (0.2Hz - 25Hz) using the software *SeismoSignal* (Boore and Bommer 2005; SeismoSoft 2012). The other recordings were obtained directly from the databases in a processed form, *i.e.* already baseline corrected and filtered. Due to the scarcity of recordings available from large magnitude subduction earthquakes, a third “*Simulated*” set, comprised of 30 simulated ground motions from subduction earthquakes with $M_w > 8.5$, is also compiled (Atkinson and Macias 2009; Mavroeidis *et al.* 2008; Sørensen *et al.* 2007; Yang 2009). The distance between the source and the site in the simulations is difficult to obtain, but most are in the range of 80-500 km. In all three sets, most of the ground motions are recorded on rock or stiff soil sites. Near-source effects are avoided in the *Crustal* set by excluding ground motions with large pulses in velocity time history as identified using the wavelet method proposed by Baker (2007). Ground motion data for all the three sets are provided in Raghunandan (2013).

The mean significant duration of the *Crustal*, *Subduction* and *Simulated* sets are 13.9s, 44.3s and 111.8s, respectively; the distribution of ground motion durations for each set is provided in Figure 16(a). The large magnitude of the subduction earthquakes (which include all the $M_w > 8$ events in the database) contributes to the longer duration of the subduction ground motions because higher moment magnitude events have a larger rupture area, which requires more time to release strain energy (Kramer 1996). The relationship between magnitude and duration also explains the longer duration of ground motions in the *Simulated* set, which represent large magnitude subduction earthquakes. Differences in source-to-site distance also affect the duration of ground motions in the database. As seismic waves travel, they scatter, thus increasing the separation in arrival times between different waves at distant sites, and increasing strong motion duration (Bommer *et al.* 2009). The subduction ground motions used in this study are recorded at large distances from the earthquake hypocenter because the geology of subduction zones is such that the rupture typically occurs at a significant distance from the built environment.

Figure 16(b) shows the mean acceleration response spectra for each of the three sets of ground motions. When all records are scaled to the same intensity at 1s to compare frequency content, the plot shows that at shorter periods, the *Subduction* motions have relatively higher intensities than *Crustal* earthquakes and at longer periods they have similar intensities (consistent with Figure 15(b)). Figure 16(b) also indicates that the *Simulated* ground motions have high energy associated with longer periods, as compared to the *Subduction* set. The primary factors contributing to the longer period energy of simulated ground motions in this study are the high magnitude of the simulated interface earthquakes at source and large source to site distance, showing the trend observed in Figure 15(a). In addition, the simulations used in this study are based on methodologies that had not yet been validated against the most recently recorded large magnitude earthquakes (e.g., M_w 9.0 Tohoku, Japan and M_w 8.8 Maule, Chile). Ghofrani *et al.* (2013) showed that Atkinson and Macias (2009) approach could be modified to ensure that simulations have lower long period energy and more closely match the newly available recordings.

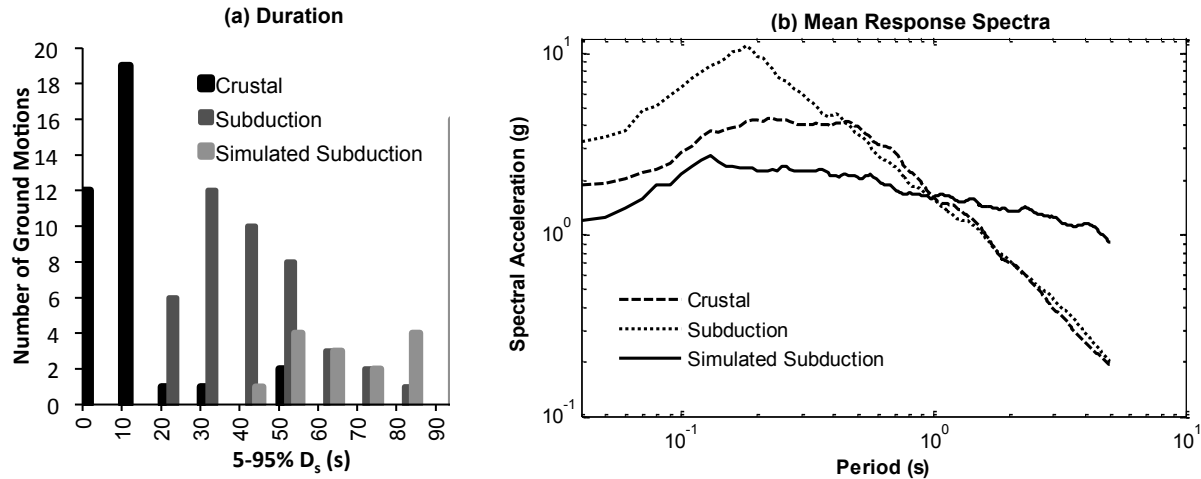


Figure 16. Characteristics of ground motions used in analysis showing: (a) distribution of 5-95% significant duration (D_s) of *Crustal*, *Subduction* and *Simulated* ground motion sets and (b) the mean response spectra for each set of ground motions. An additional 16 of the *Simulated* records have $100s < 5-95\% D_s < 450s$ (not plotted). Some ground motions have relatively low PGAs, such that the 0.05g bracketed durations are between 0s and 247s. In (b) response spectra are scaled to 1.6g at 1s.

3. Seismic Design History of the Pacific Northwest

In order to understand the collapse risk of existing and modern buildings in the Pacific Northwest, it is important to provide a brief history of seismic design there. The cities of Seattle and Portland adopted municipal seismic provisions in 1946 and 1953, respectively (Don 2007; EERI 2005). By the 1960s or early 1970s, these local seismic provisions were replaced by statewide adoption of the Uniform Building Code (UBC) and, in the 2000s, the International Building Code (IBC).

Figure 17 highlights the major changes in seismic design that have occurred in Portland and Seattle, looking at the variation of seismic design forces for 2, 4 and 8-story RC frame buildings. In particular, it shows how the design base shear has changed to reflect improved understanding of the seismic hazard in the Pacific Northwest. In older codes, sites were divided into seismic zones. Prior to 1976, Seattle, like Los Angeles, was classified in the highest seismic zone (zone 3) because of the occurrence of the 1949 and 1965 Olympia intraslab earthquakes. In the 1976 UBC, Los Angeles was upgraded to a new, higher seismic zone 4. Due to lack of knowledge of the Cascadia subduction hazard, Portland was assigned to zone 2. The seismic hazard associated with the Cascadia subduction zone was acknowledged in the 1980s (Heaton and Kanamori 1984). It first appears in seismic design codes in the 1994 UBC, producing an increase in design forces in Portland and Seattle. The change was more dominant for Portland because it upgraded the city from zone 2B to 3, the same as Seattle. With the adoption of the 2000 IBC, the seismic zonation concept was replaced with ground motion maps based on probabilistic and deterministic seismic hazard analysis, considering both crustal and subduction sources (Leyendecker et al. 2000).

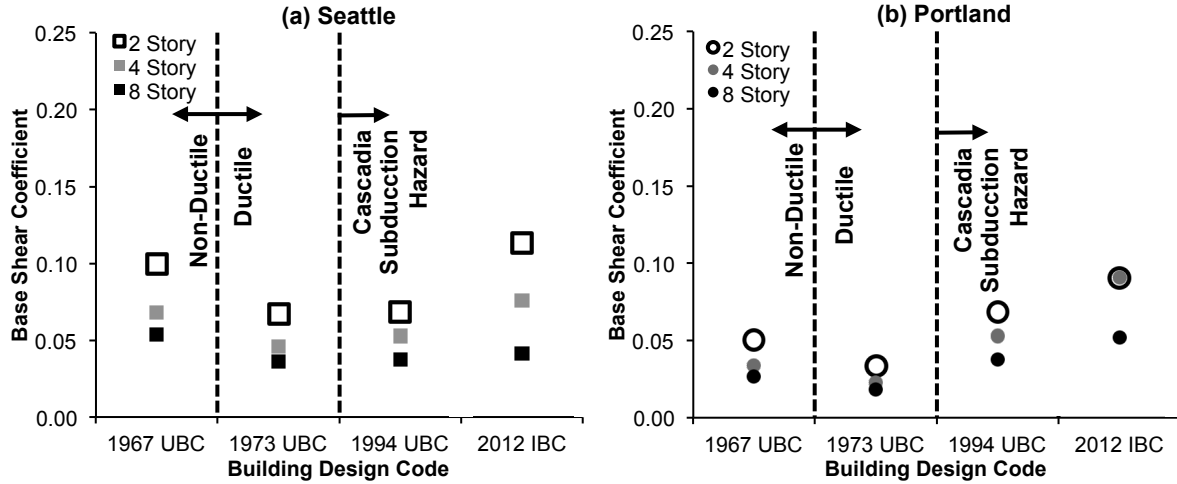


Figure 17. History of the seismic design base shear coefficient (V_{design}/W) for buildings in (a) Seattle, and (b) Portland. The figure is annotated to show the significant changes in design and detailing occurring around 1973 and 1994. For the calculation of design base shear coefficient, the fundamental period is estimated based on approximate equations given in the respective building code and all buildings are assumed to be on site class D (stiff soils).

Another major change in seismic design in the last 50 years has been the implementation of ductile detailing requirements for RC frames (as well as complementary requirements for other structural systems). For RC frames, ductile detailing provisions were instituted in the early 1970s in response to the poor performance of non-ductile concrete buildings in the 1971 San Fernando and other earthquakes (Moehle 1998). Prior to 1973, ductile moment frames were required only for concrete or steel frame buildings taller than 160ft. In 1973, it became mandatory for concrete space frames that are part of the lateral load resisting system in seismic zones 2 or 3 to be ductile and moment resisting. This change is shown in Figure 17 by the left-most vertical dashed line, which demarcates two groups of existing buildings: (1) non-ductile frames constructed prior to 1973, and (2) ductile frames with more transverse reinforcement and higher deformation capacity constructed since 1973. Compared to the 1967 UBC buildings, the ductile 1973 UBC frames are designed for the same level of expected seismicity, but the 1973 design forces are multiplied by 0.67 because the code allows for reduction of design forces due to increased deformation capacity of ductile moment resisting structural frames. The other changes associated with detailing requirements are not directly shown in the design coefficients in Figure 17. For example, post 1970s ductile moment frames also have more closely spaced transverse reinforcement, and satisfy principles of capacity design to prevent brittle sudden failure modes. The concept of ductile detailing has remained since 1973, although the specifics have evolved over time.

4. Archetype Building Designs and Models

To assess the collapse risk of structures in the Pacific Northwest, 2, 4 and 8-story RC buildings are designed according to the four different design codes for sites in Seattle (47.6°N, 122.3°W) and Portland (45.5°N, 122.65°W), resulting in 12 buildings designed for each site. Based on the seismic history described above, the authors elected to design buildings according to (1) the 1967 UBC (ICBO 1967), (2) the 1973 UBC (ICBO 1973), (3) the 1994 UBC (ICBO 1994) and (4) the current 2012 IBC (ICC 2012) (equivalent to ASCE 7 (ASCE 2010), ACI 318 (ACI 2008)) to mark the major changes in seismic design and detailing requirements. An additional 12 buildings are designed for Los Angeles (34.05°N, 118.25°W) to compare the structural response of buildings in Portland and Seattle to buildings in a high seismic region with only crustal earthquakes. RC frames are relatively prevalent in the cities of Portland and Seattle. According to EERI (2005), in the Seattle region, concrete frames were a popular form of construction starting in the early 1940s, especially for taller (>8 stories) buildings. Likewise, OSSPAC

(2013) and Don (2007) indicate that concrete frames have been commonly built in Oregon, especially for healthcare buildings, community colleges and government facilities.

The seismic design parameters for the three cities and properties of the resulting building designs are provided in Table 4. Buildings are designed for gravity and earthquake loads; wind loads are assumed to not govern the design. All buildings are designed as space frames, with 20 foot column spacing and story heights of 13 feet (upper stories) and 15 feet (first story), as shown in Figure 18. According to USGS (2012a), most of the sites in the central areas of Portland and Seattle have NEHRP site class C (i.e., very dense soil and soft rock) or D (i.e., stiff soil). In this study, all 2012 buildings are designed for site class D. For the 1994 UBC buildings, a similar soil profile, S2, is assumed, which corresponds to medium dense to dense soil conditions. In the 1967 and 1973 UBC, soil conditions are not required for calculation of design forces. In Seattle, basin effects will amplify the ground motions at 1-5 seconds in addition to the amplification expected from shallow soils (Frankel *et al.* 2002). Currently, this basin amplification is not part of typical code designs, and is not considered in design of the Seattle buildings here. For the modern buildings, the design spectral values at all sites are governed on the risk-targeted values, not the deterministic cap that USGS (2012a) defines affecting some locations.

Table 4. Seismic design characteristics of archetype buildings for each city and era.

	City	Stories	Seismic Hazard ^[1]	DBS Coefficient ^[2]	T ₁ ^[3]	μ ^[4]	Ω ^[5]
1967 UBC: NDMRF ^[6]	Seattle	2	Zone 3	0.100	0.70	4.0	2.9
		4		0.068	1.11	3.5	2.9
		8		0.054	2.02	3.0	1.7
	Portland	2	Zone 2	0.050	0.70	4.3	5.8
		4		0.034	1.29	2.9	4.3
		8		0.027	2.30	2.9	2.8
	Los Angeles	2	Zone 3	0.100	0.70	4.0	2.9
		4		0.068	1.11	3.5	2.9
		8		0.054	2.02	3.0	1.7
1973 UBC: DMRF ^[6]	Seattle	2	Zone 3	0.067	0.65	13.0	5.6
		4		0.045	1.07	8.9	4.2
		8		0.036	1.88	6.2	2.9
	Portland	2	Zone 2	0.033	0.65	15.0	10.7
		4		0.023	1.21	7.5	7.0
		8		0.018	2.17	7.8	4.5
	Los Angeles	2	Zone 3	0.067	0.65	13.0	6.0
		4		0.045	1.07	8.9	4.2
		8		0.036	1.88	6.2	2.9
1994 UBC: SMRF-1 ^[6]	Seattle	2	Zone 3	0.069	0.60	14.7	5.9
		4		0.053	0.99	10.7	4.3
		8		0.038	1.79	7.8	3.1
	Portland	2	Zone 3	0.069	0.60	14.7	5.9
		4		0.053	0.99	10.7	4.3
		8		0.038	1.79	7.8	3.1
	Los Angeles	2	Zone 4	0.092	0.56	15.8	5.1
		4		0.070	0.95	10.7	3.5
		8		0.050	1.64	8.8	2.7
2012 IBC: SMRF-2 ^[6]	Seattle	2	S _s =1.37g S ₁ =0.53g	0.114	0.58	14.5	3.9
		4		0.081	1.00	11.3	2.7
		8		0.044	1.80	9.5	2.3
	Portland	2	S _s =0.98g S ₁ =0.42g	0.091	0.63	14	4.2
		4		0.068	1.00	12.4	3.1

		8		0.037	1.98	7.8	2.5
	Los	2	$S_s=2.40g$ $S_1=0.84g$	0.200	0.54	13.6	2.7
	Angeles	4		0.130	0.86	12.8	2.4
		8		0.071	1.57	9.6	2.0

^[1] Seismic hazard information is provided in terms of seismic zones for the 1967- 1994 buildings. For the 2012 buildings, the seismic hazard is reported in terms of the risk-targeted Maximum Considered Earthquake (MCE_R) ground motion response spectra value at $T = 0.2s$ (S_s) and $T = 1s$ (S_1) at the site.

^[2] Design base shear coefficient calculated as the ratio of the design base shear to the building weight.

^[3] First-mode (fundamental) period from eigenvalue analysis, considering cracked concrete sections.

^[4] Ductility capacity computed as the ratio of ultimate displacement to the effective yield displacement calculated from the nonlinear pushover analysis of the building (FEMA 2009).

^[5] Overstrength ratio calculated as the ratio of maximum base shear of the building from nonlinear static pushover analysis to the design base shear.

^[6] Seismic detailing criteria for buildings designed. Details are provided in the text.

The buildings can be grouped into two major categories according to their deformation capacities. The non-ductile buildings (identified as NDRMF in Table 4) are designed according to the 1967 UBC and represent older buildings that have inadequate deformation capacity due to poor reinforcement and detailing. These buildings may be susceptible to shear and axial failure in columns and other brittle failure modes. As shown in Table 4, these buildings have low ductility capacities and overstrengths. Buildings designed in 1973 or later are referred to as ductile moment resisting frames, although the exact provisions vary depending on the design era of interest. The main difference between the ductile moment resisting frames (DMRF), and the special moment resisting frames (SMRF) is the strong column-weak beam requirement, which prevents or delays the formation of story mechanisms. Specifically, the DMRF has columns that are at least as strong as beams, whereas the SMRF requires columns that are at least 20% stronger than beams. This difference in the strong column-weak beam requirement, the absence of capacity design requirements for shear design and other differences in detailing regulations explain the relatively lower overstrengths and ductility capacities observed for the 1973 buildings. SMRF design, which refers to the buildings designed according to the 2012 IBC and 1994 UBC, is controlled by strong column-weak beam requirements, capacity design provisions preventing column shear failure, detailing requirements for transverse reinforcement and lap splices, and story drift limits. There are, however, minor differences in transverse reinforcement spacing requirements in buildings designed according to the 1994 UBC (denoted SMRF-1) and those designed according to modern codes (SMRF-2). These factors contribute to the slightly greater overstrength of the SMRF-1s as compared to the SMRF-2 buildings.

5. Nonlinear Simulation Models

All buildings are modeled in the *OpenSees* (2012) software as two-dimensional, three bay, space frames as shown in Figure 18. The nonlinear models must be capable of capturing different modes of strength and stiffness deterioration and component failure to successfully simulate structural collapse. The models used in this study use plastic hinges to describe the flexural behavior of beam-column members. The plastic hinges are modeled using the hysteretic material model developed by Ibarra *et al.* (2005), which can simulate the strength and stiffness deterioration due to hysteresis under dynamic loading. The material properties for the plastic hinges, such as strength, cracked stiffness, and deformation capacity, and cyclic degradation, are calculated using empirical relationships obtained by calibrating the model to experimental tests of more than 250 RC columns (Haselton *et al.* 2008). The resulting modeled properties of the beam-column plastic hinges vary depending on the column design and detailing, and account for bond slip between rebar and concrete.

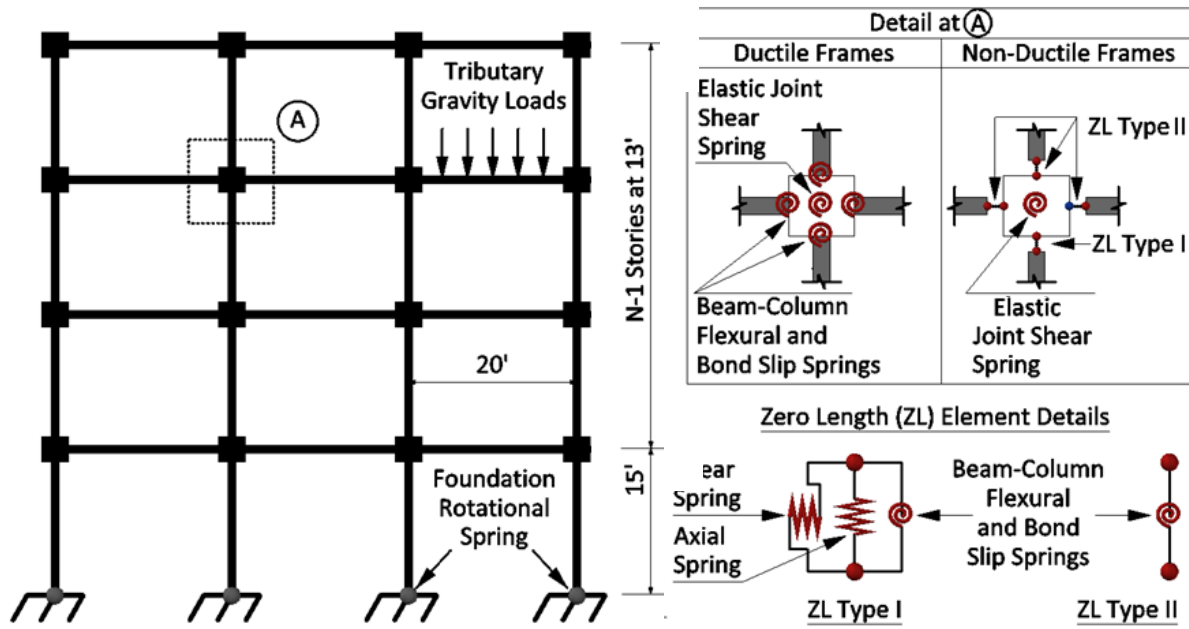


Figure 18. Graphical representation of the analytical building model.

The non-ductile buildings may be vulnerable to collapse due to column shear failure and subsequent loss of gravity-load bearing capacity, which cannot be captured by previously-described lumped plasticity beam-column element. Therefore, for the 1967 buildings, zero-length uniaxial shear and axial springs are employed along with the rotational spring at the top of the columns, as detailed in Figure 18. These springs are provided only at the top of each element, since they represent the shear and axial response over the height of the column in an average sense (Elwood 2004); failure of the spring represents shear or axial failure somewhere within the column. The model for shear and axial failure tracks the flexural response of the associated beam-column element, detecting axial and shear failure when the response reaches pre-defined shear and axial limit surfaces. These limit surfaces are determined based on the properties of the columns. In the case of shear failure, the limit surface is defined in the small displacement range, for brittle shear failure, by the shear strength model proposed by Sezen and Moehle (2004); in the larger displacement range, for a column that yields in flexure then fails in shear, the limit surface is defined by the force-displacement relationship proposed by Elwood (2004). The axial force-displacement limit surface is defined by Elwood (2004). Once the response reaches the limit surface, the properties of the respective shear and axial springs are updated to represent the expected negative slope of the element (Baradaran Shoraka and Elwood 2013).

Flexible foundations are modeled by employing elastic, semi-rigid rotational springs at the base of ground floor columns. Elastic joint shear springs are assigned to the center node of the 2D panel zone to represent joint shear flexibility and shear deformation of the joint panel. The model captures geometric nonlinearities ($P-\Delta$ effects). The modeled seismic mass represents the weight of the building tributary to the space frame of interest. Rayleigh damping of 5% is assigned to the first and third modes of each structure.

6. Building Collapse Simulation

Incremental dynamic analysis (IDA) is carried out on each building model to measure the seismic response of the structure (Vamvatsikos and Cornell 2002). In IDA, a building model is subjected to a ground motion of interest, and the structural response is simulated. The ground motion is then scaled to a higher intensity and reapplied to the original model. This process of scaling the ground motion continues until the analysis indicates the structure collapses. The analysis is then repeated for other ground motions.

In the nonlinear dynamic analyses in this study, collapse occurs when (a) interstory drifts increase without bounds due to large flexural deformations in beams and columns (“sidesway” collapse), (b) the total story shear capacity becomes less than the residual story shear capacity at any story, or (c) the gravity load demand in a story exceeds the total axial capacity of columns in that story. Sidesway collapse due to large interstory drifts is the expected collapse mode for ductile moment frames (Haselton *et al.* 2011). The global failure criteria (b) and (c) are used to identify when brittle shear or axial failure in a sufficient number of columns causes collapse of a story in the non-ductile frames. These criteria are similar to those proposed by Baradaran Shoraka (2013). The residual story shear capacity is calculated as the sum of residual capacities of columns for that story (a low residual column capacity value is assumed, about 5% of column strength). Due to challenges with model convergence, collapse mode (b) is also triggered if the shear capacities of 75% or more of the columns in any story have deteriorated to the residual level. In the case of global vertical collapse mode (c), the column axial demand is calculated from the vertical (gravity) forces acting on the structure. Before axial failure is triggered, the column axial capacity is calculated based on the axial limit surface proposed by Elwood (2004). Once the column response hits the axial limit surface, the column axial capacity is taken as zero.

A significant consideration when conducting IDAs is the choice of measure to quantify the intensity of the ground motion (referred to as an “intensity measure” or IM). Two possible IMs are the elastic spectral acceleration at a building’s fundamental period, $S_a(T_1)$, and the inelastic spectral displacement at the fundamental period, S_{di} . $S_a(T_1)$ is one of the most commonly used IMs. It does not, however, reflect the spectral shape of the ground motion, which can significantly influence nonlinear structural response (Baker and Cornell 2006; Haselton *et al.* 2011). Consequently, S_{di} is used primarily in this study. S_{di} is defined as the maximum displacement of a single-degree-of-freedom oscillator with bilinear behavior (Tothong and Luco 2007). The oscillator has the same period as the fundamental period of the building of interest, a defined yield displacement, d_y , and assumed 5% post-yield hardening stiffness ratio. In this study, d_y is calculated from pushover analysis of the building (see Table 4). The value of S_{di} reflects both the intensity and shape of the ground motion spectrum, due to period elongation of the oscillator that makes it respond to different regions of the spectrum. Although S_{di} cannot capture higher mode effects, its use reduces biases in structural response associated with the scale factor applied to the record in the analysis (Tothong and Luco 2007). This robustness in the face of ground motion scaling is important, since there is a scarcity of rare ground motions large enough to cause structural collapse. It is worth recalling, however, that USGS (2012a) quantifies seismic hazard through $S_a(T_1)$. The use of a common IM for quantifying structural response and hazard is required for calculation of an annualized probability of collapse of a structure at a particular site.

Figure 19(a) illustrates IDA results for the 2-story Los Angeles building designed according to the 2012 IBC. The collapse capacity of the structure is quantified by the ground motion intensity at which collapse occurs for each of the different ground motions. These results are used to compute the median and dispersion of the collapse capacity, where the median collapse capacity $S_{di} = 9.5$ in corresponds to the ground motion intensity that has a 50% probability of causing collapse of the building. The uncertainty in the collapse capacity is due to record-to-record variability in structural response quantified by the logarithmic standard deviation (0.36 in this case).

7. Collapse Results

7.1 Collapse Fragility of Archetype Buildings

To quantify the collapse safety of a building on being subjected to crustal and subduction records, collapse fragility curves for each earthquake type are generated from the IDA results. Table 5 summarizes the collapse capacities for all of the buildings and earthquake types in terms of the median S_{di} causing

collapse (denoted \hat{S}_{di}).² Figure 19(b) presents collapse fragility curves calculated separately for the *Crustal* and *Subduction* ground motion sets for the Portland, Seattle and Los Angeles 2-story modern buildings. These results show a reduction in median collapse capacity when subjected to *Subduction* rather than *Crustal* ground motion records. This observation implies that, for a given level of ground motion intensity, the probability of collapse for these 2-story buildings is lower if the ground shaking comes from a crustal earthquake than if it comes from a subduction earthquake.

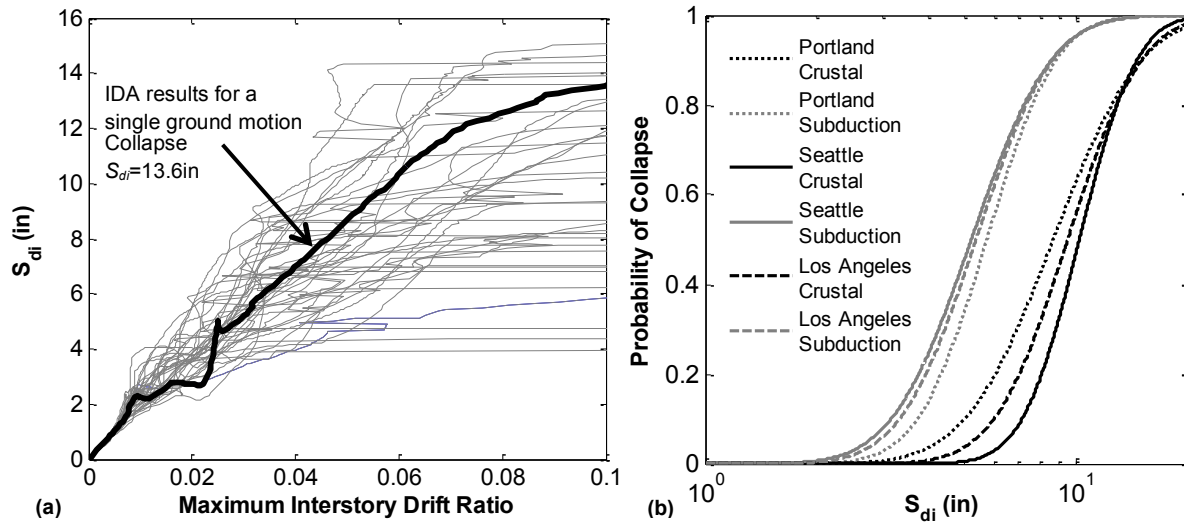


Figure 19. (a) IDA results for the 2-story Los Angeles building designed according to the 2012 IBC and subjected to the *Crustal* ground motions. (b) Collapse fragility curves developed for 2-story buildings designed according to the 2012 IBC in Portland, Seattle and Los Angeles for the *Crustal* and *Subduction* ground motion sets.

Figure 20 illustrates results for more of the buildings, revealing consistently higher fragility (lower collapse capacity) when subjected to the *Subduction* rather than *Crustal* motions. Interestingly, on average, the median collapse capacity of the most ductile (2012 IBC) buildings is reduced by 36% when subjected to *Subduction* set as compared to the *Crustal* set, whereas only 12% reduction is observed for non-ductile buildings. Presumably, the gap between collapse capacities under *Subduction* and *Crustal* motions is wider for the more ductile buildings due to the effect of ground motion duration. For ground motions having the same S_{di} , longer duration ground motions tend to be more damaging to structures, due to the larger number of load reversal cycles and larger hysteretic energy demand on the structure. However, for structures with smaller deformation and hysteretic energy capacities, duration is less important because even a short duration record is able to exhaust the structure's capacity (Raghunandan and Liel 2013). Thus, the rate of reduction in collapse capacity with duration is higher for ductile buildings as compared to non-ductile buildings.

Table 5. Collapse fragility parameters for all archetypical buildings subjected to *Crustal*, *Subduction* and *Simulated* subduction ground motion sets.

City	Stories	Design Bldg. Code	<i>Crustal</i> (C)			<i>Subduction</i> (S)			<i>Simulated</i> (Si)		% Variation in \hat{S}_{di}		
			\hat{S}_{di} (in)	β [2]	$\hat{S}_a(T=1)$ (g) [3]	\hat{S}_{di} (in)	β	$\hat{S}_a(T=1)$ (g)	\hat{S}_{di} (in)	β	C vs. S [4]	C vs. Si	S vs. Si
Seattle	2	1967	4.2	0.29	0.63	3.6	0.28	0.62	2.8	0.36	13%	33%	23%
	2	1973	10.6	0.30	1.62	7.1	0.29	1.26	4.2	0.46	33%	60%	40%
	2	1994	9.9	0.32	1.62	6.0	0.33	1.13	4.2	0.50	40%	58%	30%
	2	2012	10.2	0.28	1.69	5.2	0.39	1.02	4.3	0.45	49%	58%	17%

² The collapse S_{di} values for a particular building are assumed to follow a lognormal distribution. The goodness-of-fit is not rejected with the Kolmogorov–Smirnov normality test at the 5% significance level.

City	Stories	Design Bldg. Code	Crustal (C)			Subduction (S)			Simulated (Si)		% Variation in \hat{S}_{di}		
			$\hat{S}_{di}^{[1]}$ (in)	$\beta^{[2]}$	$\hat{S}_a(T=1)$ (g) ^[3]	\hat{S}_{di} (in)	β	$\hat{S}_a(T=1)$ (g)	\hat{S}_{di} (in)	β	C vs. S ^[4]	C vs. Si	S vs. Si
	4	1967	6.9	0.27	0.69	5.9	0.24	0.64	5.1	0.25	15%	26%	14%
	4	1973	14.3	0.35	1.61	8.6	0.23	1.19	6.9	0.24	40%	52%	20%
	4	1994	14.9	0.36	1.67	8.4	0.28	1.04	6.6	0.39	44%	56%	22%
	4	2012	14.9	0.37	1.66	8.4	0.30	1.02	6.5	0.39	44%	57%	23%
	8	1967	9.2	0.18	0.65	7.7	0.23	0.55	7.8	0.27	17%	16%	-2%
	8	1973	19.9	0.22	1.72	14.2	0.32	1.48	12.7	0.29	29%	36%	10%
	8	1994	23.1	0.21	1.79	16.8	0.36	1.41	13.4	0.34	28%	42%	20%
	8	2012	20.5	0.27	1.56	14.1	0.32	1.16	12.8	0.34	31%	38%	9%
Portland	2	1967	4.3	0.30	0.64	3.7	0.26	0.63	2.8	0.37	13%	34%	24%
	2	1973	11.0	0.32	1.67	7.5	0.26	1.32	4.3	0.48	32%	61%	42%
	2	1994	9.9	0.32	1.62	6.0	0.33	1.13	4.2	0.50	40%	58%	30%
	2	2012	8.7	0.43	1.48	5.8	0.34	1.05	4.1	0.43	34%	52%	28%
	4	1967	6.8	0.23	0.62	6.3	0.28	0.59	5.1	0.21	8%	25%	19%
	4	1973	13.9	0.37	1.23	9.2	0.26	0.83	6.6	0.27	34%	52%	28%
	4	1994	14.9	0.36	1.67	8.4	0.28	1.04	6.6	0.39	44%	56%	22%
	4	2012	14.9	0.37	1.66	8.5	0.30	1.03	6.8	0.37	43%	54%	19%
	8	1967	9.0	0.20	0.60	8.1	0.31	0.54	3.0	0.40	10%	67%	63%
	8	1973	20.1	0.22	1.18	15.1	0.30	0.88	13.9	0.29	25%	31%	8%
	8	1994	23.1	0.21	1.79	16.8	0.36	1.41	13.4	0.34	28%	42%	20%
	8	2012	22.3	0.23	1.61	15.8	0.32	1.22	14.0	0.27	29%	37%	11%
Los Angeles	2	1967	4.3	0.30	0.63	3.7	0.26	0.62	2.8	0.37	13%	34%	24%
	2	1973	11.0	0.32	1.62	7.5	0.26	1.26	4.3	0.48	32%	61%	42%
	2	1994	10.1	0.29	1.74	5.3	0.40	1.09	4.3	0.41	48%	57%	18%
	2	2012	9.5	0.36	1.73	5.4	0.37	1.19	4.3	0.36	43%	55%	21%
	4	1967	6.8	0.23	0.69	6.3	0.28	0.64	5.1	0.21	8%	25%	19%
	4	1973	13.9	0.37	1.61	9.2	0.26	1.19	6.6	0.27	34%	52%	28%
	4	1994	14.1	0.30	1.64	8.2	0.30	1.02	6.4	0.41	41%	54%	22%
	4	2012	14.9	0.35	1.89	9.1	0.35	1.21	6.4	0.45	39%	57%	30%
	8	1967	9.0	0.20	0.65	8.1	0.31	0.55	3.0	0.40	10%	67%	63%
	8	1973	20.1	0.22	1.72	15.1	0.30	1.48	13.9	0.29	25%	31%	8%
	8	1994	23.5	0.24	1.88	16.2	0.33	1.39	12.9	0.31	31%	45%	20%
	8	2012	22.0	0.24	1.79	14.8	0.37	1.30	12.5	0.36	33%	43%	16%

^[1] Median collapse capacity quantified in terms of S_{di} in units of inches.

^[2] Logarithmic standard deviation of collapse capacity when intensity is quantified in terms of S_{di} .

^[3] Median collapse capacity quantified in terms of $S_a(T=1s)$ in units of g.

^[4] The percent difference of A vs. B is computed as $100 \cdot (A-B)/A$.

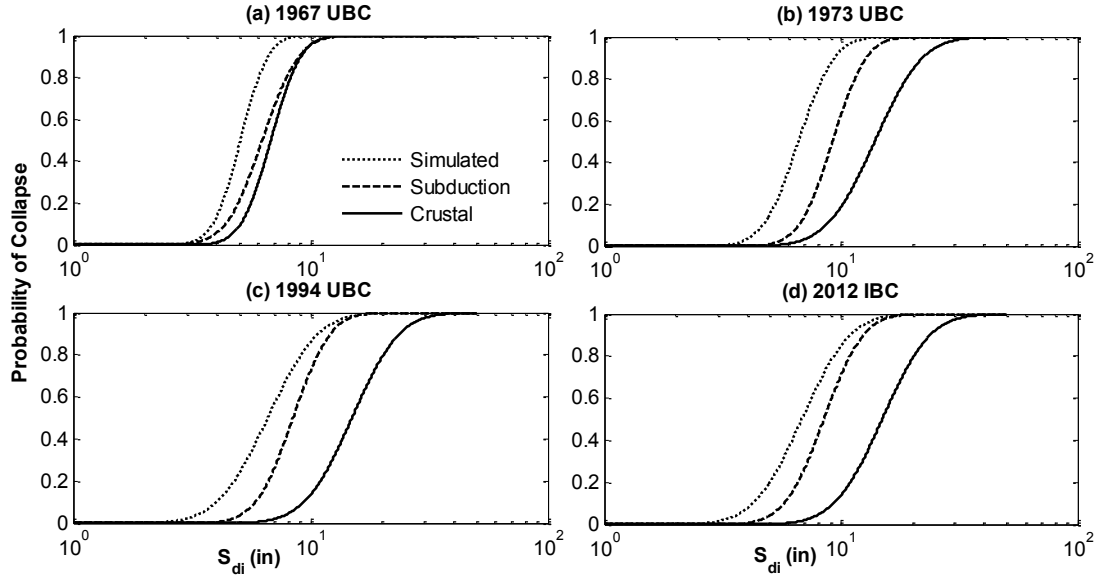


Figure 20. Collapse fragility curves developed for 4-story buildings designed according to 1967 UBC, 1973 UBC, 1994 UBC and 2012 IBC in Portland, showing increasing discrepancy between response to subduction and crustal motions for the newer, more ductile buildings.

With regard to the comparison between the simulated versus recorded subduction ground motions, the building collapse capacities measured under the *Simulated* subduction motions are around 24% lower than those obtained with the recorded *Subduction* motions. This difference is due to two factors. First, on average, the *Simulated* ground motions have 2.5 times longer duration than the *Subduction* set, causing more damage to the structures. In addition, the higher energy of the *Simulated* ground motions at longer periods results in larger seismic forces imposed on a structure as its period elongates due to structural damage.

For comparison between buildings across cities and design eras, and for computing the annualized risk of collapse, the median collapse capacity is also quantified in terms of $S_a(T=1s)$ for all buildings in Table 5. The S_{di} values cannot be easily employed for comparison between buildings because of different periods and yield displacement. Although not reported, there is a general increase in the record-to-record variability of collapse fragility curves with $S_a(T=1s)$ as compared to S_{di} because the former does not account for spectral shape effects and uses a common period (1s) in the calculations. As detailed in Table 5, among the non-ductile buildings (1967 UBC), all of the buildings with the same number of stories have similar collapse capacities, regardless of building location, because the dominant collapse mode for these buildings is shear and axial failure of the columns, and all buildings had similar column sizes and spacing of transverse reinforcement. For the first generation ductile buildings (1973 UBC), the Los Angeles and Seattle buildings have the larger collapse capacities than the Portland buildings due to the differences in design seismic zone. However, with the increase in seismic design forces for Portland buildings due to the inclusion of the Cascadia subduction hazard in 1994, the design forces and, hence, collapse capacities are identical for the Portland and Seattle buildings. The Los Angeles 1994 buildings have higher collapse capacities because they are designed for larger design forces. Among the 2012 IBC buildings, the design forces are lowest for Portland and largest for Los Angeles. Accordingly Los Angeles has the highest collapse capacity. The Seattle and Portland buildings' collapse capacities are very similar because of minimum reinforcement and strong column-weak beam requirements.

On average, the $\hat{S}_a(T=1s)$ results suggest that median collapse capacities, computed based on the *Crustal* results, improved by a factor of 2.6 (average) between the 1967 and 2012 codes. Most of this improvement was achieved by the introduction of ductile detailing requirements in 1973; in fact, the 1973

buildings have, on average 2.4 times better collapse capacities than the 1967 buildings. Note, however, that the collapse capacities of the most ductile buildings are likely underestimated because the unique spectral shape of rare ground motions was not considered in ground motion selection and is not captured by $Sa(T=1s)$ (Haselton *et al.* 2011b). As a result, the difference between the 1967 and 2012 buildings is likely closer to a factor of 3 on the median collapse capacity.

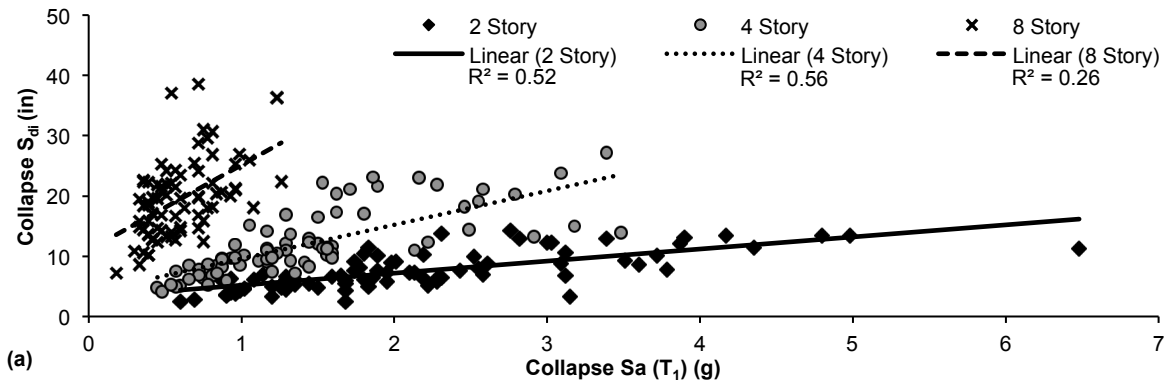
6.2 Influence of Ground Motion Parameters on Collapse Capacity

Previous research demonstrates that ground motion frequency content and duration both strongly influence structural response. This section investigates the role of each of these parameters in the observed trends in collapse capacity.

Ground Motion Frequency Content

We hypothesize that part of the decrease in collapse capacity associated with the subduction records is due to the differences in frequency content between the crustal and subduction ground motions (Figures 15 and 16). Indeed, the primary objective of employing S_{di} as an IM is to quantify the combined effect of ground motion intensity and spectral shape on structural response. Since the period of the bilinear oscillator used to calculate S_{di} elongates during response, the oscillator “feels” the spectral intensity of the ground motion at periods greater than T_1 . Therefore, the collapse capacities expressed in terms of S_{di} already account for the influence of differences in spectral shape between *Crustal* and *Subduction* motions.

To illustrate this point, Figure 21 plots the variation of collapse S_{di} with: (a) an IM that measures spectral intensity at a single period, $Sa(T_1)$, and (b) an IM that captures the influence of spectral shape, S^* . S^* , proposed by Cordova *et al.* (2000), quantifies ground motion intensity and spectral shape by incorporating the spectral acceleration at two periods, T_1 and $2T_1$: $S^* = Sa(T_1)\sqrt{Sa(2T_1)/Sa(T_1)}$. These IMs are compared by quantifying the value of each IM that caused collapse of the modern 2, 4, and 8-story Portland buildings for each ground motion. Figure 21 indicates that there is stronger correlation (indicated by modestly higher R^2 values of the linear regression, where R^2 is the square of the linear correlation coefficient) between S^* and S_{di} , as compared to $Sa(T_1)$ and S_{di} , demonstrating that S_{di} is able to capture the longer period spectral shape effects through period elongation. The correlations are slightly lower for the 8-story building, since collapse is sensitive to higher mode effects not captured by any of the IMs.



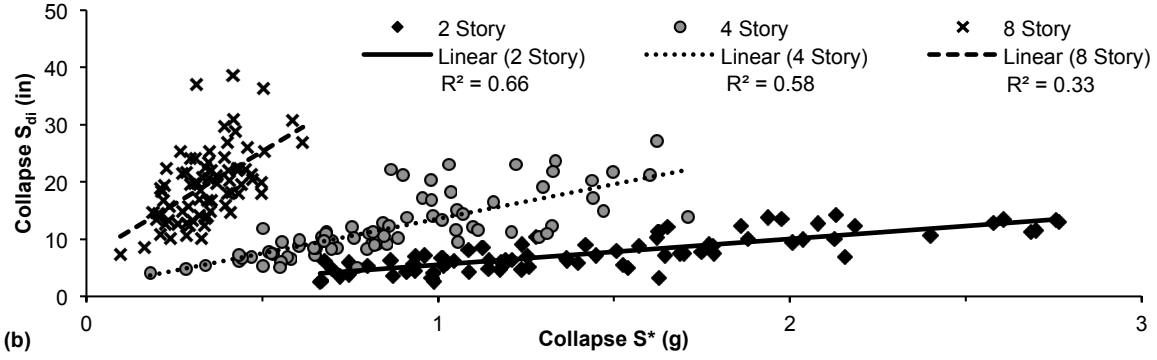


Figure 21. Variation of S_{di} with (a) $Sa(T_1)$ and (b) S^* (Cordova *et al.* 2000) at collapse of 2, 4, and 8-story Portland buildings designed according to the 2012 IBC.

The suitability of S_{di} as a predictor of nonlinear structural response is further supported by comparison of the lognormal standard deviations of the collapse capacities, β , computed in terms of the different IMs. β provides a measure of the efficiency of an IM, since lower record-to-record variability in response indicates that the IM better captures those characteristics of ground motions that are important for collapse behavior. Based on the IDA results for the same buildings on being subjected to the combined *Crustal* and *Subduction* sets, $Sa(T_1)$ has the highest β (0.50, 0.48, 0.38). β is lower when S_{di} (0.43, 0.44, 0.33) or S^* (0.38, 0.42, 0.32) are used as IMs. Similar trends are obtained for the buildings designed for other cities and code eras.

These observations are used to make inferences about the role of ground motion frequency content on building collapse in the Cascadia subduction zone. Referring back to Table 5, results show that the percentage difference between the median collapse capacities computed in terms of S_{di} from subduction versus crustal records is greater than the percentage difference between the median collapse capacities computed in terms of $Sa(T=1s)$. It is hypothesized that the S_{di} collapse capacities are picking up on the differences in frequency content between the crustal and subduction records, finding that the subduction records are even more damaging (relative to crustal records) than would be predicted based on $Sa(T_1)$.

Ground Motion Duration

Ground motions with longer duration are more damaging to structures. Since S_{di} accounts for differences in frequency content, ground motion duration is hypothesized to be the primary reason for the observed reduction in collapse capacity between the *Crustal* and *Subduction* ground motions. To test this hypothesis, the generalized linear regression model (GLM) developed by Raghunandan and Liel (2013) is used to predict the collapse capacity of each building when subjected to each of the ground motion records. The GLM model takes as input (1) ground motion duration and (2) structural parameters related to the building fundamental period and deformation capacity, and provides the predicted collapse capacity in S_{di} as output.

Figure 22 plots the collapse S_{di} obtained from nonlinear dynamic analysis (“Actual S_{di} ”) against the GLM model predictions (“Estimated S_{di} ”). In Figure 22(a), the results for all buildings are scattered more or less symmetrically around the 45° line, indicating that the estimates for S_{di} from the GLM model are similar to the observed value for most of the buildings and that the ground motion duration parameter has significant explanatory power for the trends observed between the *Crustal* and *Subduction* dynamic analysis results. However, some data points are substantially offset from the 45° line for both *Crustal* and *Subduction* records. Closer evaluation of results for individual buildings in Figure 22(b) and (c) reveals that this bias occurred mainly for the taller (8-story) buildings. This observation confirms that higher mode effects that are important predictors of collapse capacity for taller buildings are not accounted for by the S_{di} and duration-based GLM model. Higher mode effects are not judged to be crucial here, since

they introduce a small and relatively consistent bias in the *Crustal* and *Subduction* collapse assessments for each building. We find no systematic bias in the actual versus estimated S_{di} values due to differences in frequency content, confirming that spectral shape issues are adequately covered by the use of S_{di} .

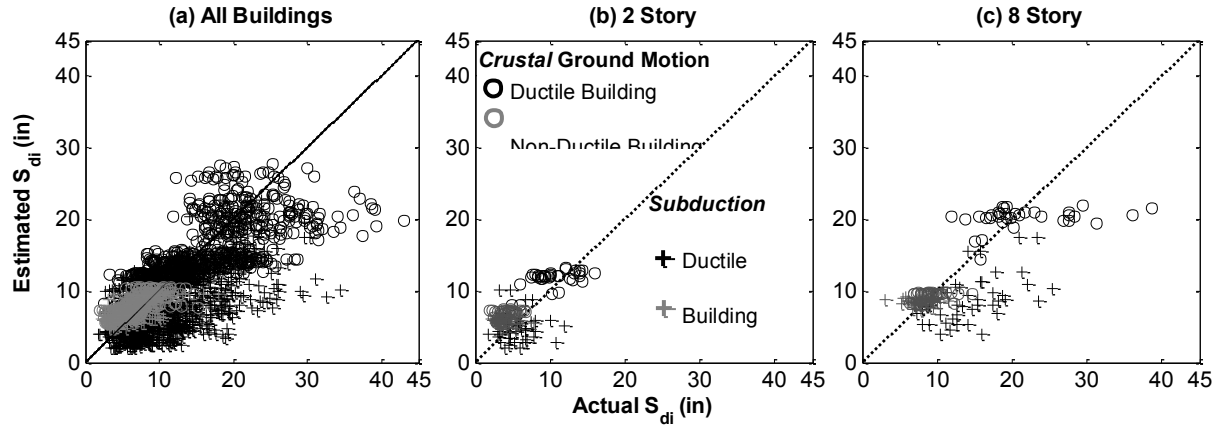


Figure 22. Comparison of “actual” collapse S_{di} from nonlinear dynamic analyses and “estimated” collapse S_{di} estimated from the GLM prediction equation developed by Raghunandan and Liel (2013).

6.3 Seismic Collapse Risk

Although probabilistic seismic hazard analysis could be conducted in terms of $S_{di}(d_y, T)$, USGS (2012a) currently produces seismic hazard curves in terms of $Sa(T)$ for pre-defined values of T . Therefore, in this study, the average annual frequency of collapse for each building is quantified using Equation (1), which convolves the seismic hazard with the collapse fragility curve, based on Cornell (1968)’s formulation, as applied more recently by Luco *et al.* (2007):

$$\lambda[\text{Collapse}] = \int_0^\infty \lambda[SA] f(c) dc \quad (1)$$

The probability of collapse in $t = 50$ years for each building can be obtained through Equation (2), assuming a Poisson distribution of earthquake occurrence in time:

$$P[\text{Collapse in 50 yrs.}] = 1 - \exp(-\lambda[\text{Collapse}] * 50) \quad (2)$$

Here, $\lambda[\text{Collapse}]$ is the mean annual collapse frequency. $\lambda[SA]$ is the annual frequency of exceedance of the spectral acceleration demand (*i.e.* seismic hazard curve), and $f(c)$ is the lognormal probability distribution of the collapse capacity, *i.e.* the derivative of the collapse fragility curve. Both the capacity (c) and the demand (SA) are quantified in terms of $Sa(T=1s)$. For consistency with previous studies, the standard deviation of the natural logarithm of collapse capacity, β , is assumed to be equal to 0.6, and considers uncertainty in design and modeling on top of record-to-record variability (ASCE 2010).

In this study, the calculations in Equation (1) and (2) are carried out separately for crustal and subduction events for each building by substituting the event-type-specific site hazard curve (Figure 23(a)) and collapse fragility curve (Figure 23(b)). Separate hazard curves were obtained from the USGS via Harmsen (2012). These separate curves were developed by deaggregating the total hazard curve for a site and then grouping the portions of the hazard associated with the different types of earthquake events. The crustal and subduction collapse frequencies are then added together to calculate the total annual collapse frequency at a site in Equation (3), which is used to calculate the total 50 year collapse probability (Equation (2)):

$$\lambda[\text{Collapse}]_{T-CS} = \lambda[\text{Collapse}]_C + \lambda[\text{Collapse}]_S \quad (3)$$

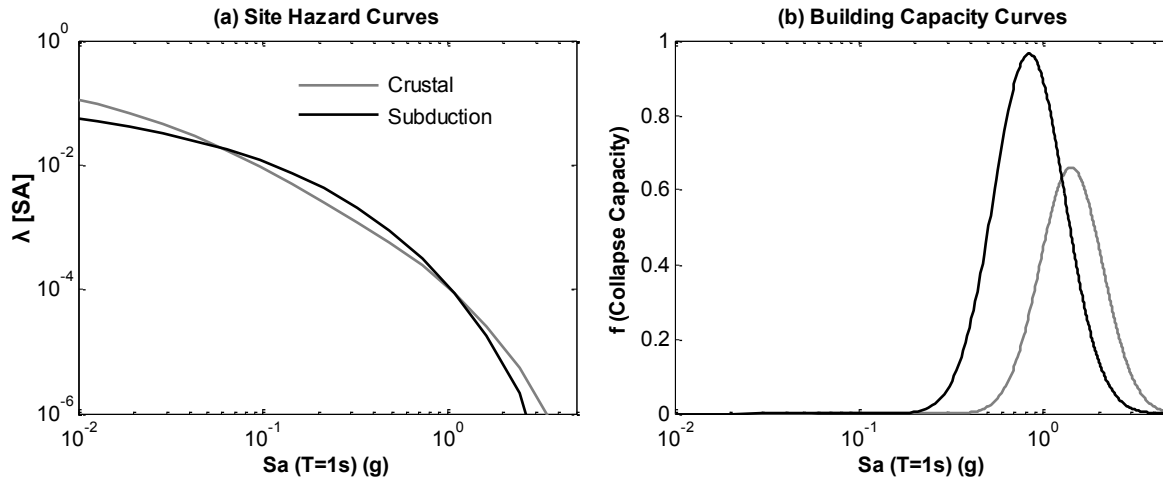


Figure 23 For Seattle: (a) event-type-specific seismic hazard curves for the selected site, assuming soil (Site Class D), and (b) collapse capacity curves (without SSF factor correction) for the 4-story building designed according to current codes (derivative of collapse fragility curve).

For the purposes of this paper, one additional modification is made before computing the annualized frequencies and 50-year probabilities of collapse. Since seismic hazard is quantified in terms of $S_a(T_1)$, to account for spectral shapes of the ground motions in the analysis and their strong influence on collapse response, the collapse fragility curves used in collapse risk calculation are multiplied by the spectral shape factor (SSF) defined in FEMA P-695 (FEMA 2009). The SSF values increase the estimated median collapse capacity ($SSF > 1$) of the structure to account for the influence of spectral shape on response and the unique spectral shape of rare, large intensity ground motions that tends to be less damaging (FEMA 2009; Haselton *et al.* 2011b). In this study, the SSF values to adjust the *Crustal* collapse capacity results are computed from FEMA P-695 and are a function of the period and ductility of the building. For adjusting the *Subduction* collapse capacity results, the same SSF s are used, even though the SSF values provided in FEMA P-695 were developed based on *Crustal* ground motions. This approach may produce a nonconservative (over) estimate of SSF for the *Subduction* collapse capacities because the longer period spectral content of the *Subduction* ground motions from high magnitude events may be particularly damaging for buildings whose periods elongate substantially before collapse.

These calculations are carried out for the three sites and all of the buildings, and the collapse risk metrics obtained are reported in Table 6 and illustrated in Figure 24. The best estimate results are labeled as T-CS for Portland and Seattle and T-C for Los Angeles (the subduction hazard is not relevant there). Deaggregating the collapse risk indicates that subduction earthquakes contribute about 60-82% of the total seismic collapse risk for buildings located in Seattle. For buildings located in Portland, subduction earthquakes are even more important, accounting for 75-91% of the collapse risk. The substantial contribution from subduction earthquakes to the collapse risk is due not only to the damaging features of the ground motions, but also to the fact that these events produce ground motions large enough to cause collapse. Since the less ductile buildings are less sensitive to the unique characteristics of subduction motions, the contribution of subduction earthquakes to the total collapse risk for these buildings is less and on the lower bound of the ranges presented above.

The usual calculation of collapse risk utilizes a seismic hazard curve representing the hazard from all sources and a building fragility curve, which is almost always developed based on solely crustal ground motions. This calculation is represented by the values labeled “T-C” in Table 6 and Figure 24. If the collapse risk calculation is carried out as in T-C, the collapse risk of the buildings at sites affected by subduction earthquakes is too low because it does not account for the higher fragility of buildings to

subduction motions. For the set of the ductile buildings (post-1970) considered here, T-C underestimates the annualized frequency of collapse, $\lambda[\text{Collapse}]$, by 50% on average. However, $\lambda[\text{Collapse}]$ is underestimated by only 10% on average in the case of the non-ductile buildings. The collapse risk of the nonductile buildings is less sensitive to the inclusion of a separate subduction fragility curve because there is not a large difference between the building capacities for the *Crustal* and *Subduction* ground motion sets.

Risk-targeted seismic design maps in current U.S. building codes define design spectral values intended to achieve a target uniform collapse probability of 1% in 50 years. This study estimates that for modern buildings designed according to the 2012 IBC, the probability of collapse in 50 years, computed considering hazard and building collapse fragilities from both crustal and subduction earthquakes, *i.e.* T-CS, is 0.30% - 0.62% in Seattle and 0.18% - 0.41% Portland. For comparison, the modern Los Angeles buildings exhibit probabilities of collapse in 50 years below 1% as well (0.34% - 0.62%). The fact that all the values fall below the 1% target value may reflect some conservatism in the design process in this study. Among the modern buildings, on average, those located in Seattle and Los Angeles exhibit the highest seismic collapse risk, followed by Portland. The relatively higher risk in Seattle could be addressed by larger MCE_R ground motion for design where the subduction risk is significant.

Table 6. Mean annual frequency of collapse values for the archetypical buildings.

Design Building Code	Stories	Mean annual frequency of collapse ($\lambda[\text{Collapse}]$) ($\times 10^{-4}$)								
		Seattle				Portland				Los Angeles
		C ^[1]	S	T-CS	T-C	C	S	T-CS	T-C	T-C
1967 UBC	2	2.78	4.20	6.99	6.95	0.97	2.91	3.89	3.80	19.33
1973 UBC	2	0.23	0.54	0.78	0.48	0.09	0.45	0.54	0.32	1.44
1994 UBC	2	0.25	0.77	1.02	0.51	0.10	0.70	0.80	0.36	1.24
2012 IBC	2	0.22	1.02	1.23	0.45	0.12	0.82	0.95	0.45	1.25
1967 UBC	4	1.99	3.37	5.36	4.85	1.07	3.48	4.55	4.18	13.60
1973 UBC	4	0.17	0.45	0.63	0.35	0.16	1.21	1.38	0.60	1.05
1994 UBC	4	0.19	0.79	0.97	0.38	0.08	0.72	0.80	0.27	1.20
2012 IBC	4	0.19	0.83	1.02	0.38	0.08	0.75	0.82	0.27	0.81
1967 UBC	8	2.27	4.91	7.19	5.61	1.10	3.94	5.05	4.29	15.67
1973 UBC	8	0.13	0.21	0.33	0.25	0.17	1.01	1.19	0.65	0.77
1994 UBC	8	0.12	0.24	0.36	0.22	0.05	0.24	0.29	0.16	0.58
2012 IBC	8	0.17	0.43	0.60	0.34	0.06	0.37	0.43	0.22	0.67

^[1] Indicates hazard curve and fragility curve used in calculation of $\lambda[\text{Collapse}]$. C: Hazard Curve-Crustal, Fragility Curve-Crustal; S: Hazard Curve-Subduction, Fragility Curve-Subduction; T-CS: Total value, combining results from crustal and subduction events as in Equation (3); T-C: Hazard Curve-Total (crustal and subduction), Fragility Curve-Crustal.

Among the buildings pre-dating modern codes, the results show that the older non-ductile buildings are at much higher risk of collapse than their ductile counterparts. On average, the probability of collapse in 50 years of the 1967 buildings is around 7.6, 7.1 and 17.8 times higher for non-ductile buildings than the modern ductile buildings for Seattle, Portland and Los Angeles, respectively. These older concrete buildings are a vulnerable component of the Pacific Northwest building stock, as they are in California and other seismically active regions (Liel and Deierlein 2012).

The subduction hazard curve used in this paper represents the combined hazard from two types of subduction earthquakes: interface (generally $M_w \geq 8$) and deep intraslab (generally $M_w < 8$) earthquakes (Atkinson and Boore 2003). The relative contribution of each type of earthquake to the total hazard varies depending on the site. Based on USGS (2012a), deaggregation of seismic hazard at $T = 1$ s for a site class *D* site at the 2% in 50 year hazard level in Seattle indicates 38% contribution from Cascadia interface earthquakes and 14% contribution from intraslab earthquakes (vis-a-vis 64% and 8% in Portland). Due to the limited number of available subduction ground motions, the authors employed a common subduction fragility curve for interface and intraslab events. In order to assess the order of influence of this

aggregation on the building vulnerability, magnitude-based building fragility curves were calculated for all the buildings using the ground motions in the *Subduction* set. For short period buildings (2 and 4-story), the median collapse capacity (quantified in terms of S_{di}) increases by 6% for large magnitude subduction earthquake ground motions ($M_w \geq 8$) as compared to smaller magnitude subduction earthquakes ($M_w < 8$); for long period buildings (8-story), the capacity decreases by 10%. These differences would not have a large influence on the annual collapse risk.

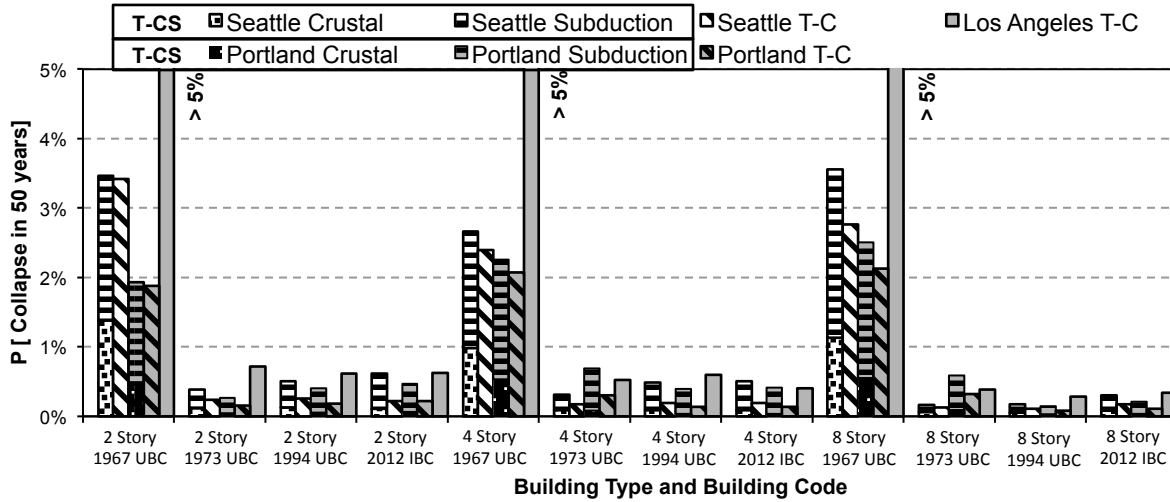


Figure 24. Probability of collapse in 50 years for all archetype buildings calculated using separate seismic hazard and building fragility curves for crustal and subduction earthquakes (T-CS) and the total seismic hazard curve and crustal building fragility curve (T-C). The T-CS results are deaggregated to show the contributions of the crustal and subduction sources to the overall collapse risk.

The collapse risk values calculated in this study do not consider the near-site directivity effects associated with crustal faults. Collapse assessment for a similar portfolio of buildings in Los Angeles by Champion and Liel (2012) showed a reduction in the collapse capacity of the buildings of up to 30% when they are subjected to near site ground motions with velocity pulses of an appropriate pulse period distribution, instead of far-field ground motions. In this study, certain sites close to Seattle fault may experience these conditions, which would be expected to result in higher total collapse risk of the building due to higher fragility for near-source crustal events.

7. Conclusions

The built environment of the Pacific Northwest region of the U.S. and Canada is at risk from both subduction and crustal earthquakes. To date, most of the research quantifying seismic building response and safety has focused on crustal, California-type ground motions. Due to the distinct characteristics of subduction earthquake sources and attenuation, however, ground motions from subduction events are different from crustal ground motions in terms of both duration and frequency content. This paper quantifies the impact of these ground motions on building response for a set of RC frame buildings designed according to 1967, 1973, 1994 and 2012 building codes and subjected to nonlinear incremental dynamic analysis. These results are used to quantify the collapse risk to provide a proxy for building safety of modern and older buildings near the Cascadia subduction zone.

The principal findings of the study are threefold. First, the median collapse capacity of the ductile and non-ductile structure reduces by, on average, 36% and 12%, respectively, when subjected to subduction ground motions as compared to crustal ground motions. This observation, which applies to buildings of various heights and designed to represent a range of building eras, suggests that a smaller intensity subduction ground motion is needed to collapse a building, compared crustal earthquake ground motion.

Both the longer duration and the distinct frequency content of ground motions from subduction earthquakes contribute to the higher susceptibility of buildings to ground shaking from subduction events.

The second finding stems from the first; due to the characteristics of building response under subduction ground shaking, the average risk of collapse of modern properly-designed buildings as quantified by the methods in this study corresponds to 0.37% probability of collapse in 50 years in Portland and 0.48% probability of collapse in 50 years in Seattle. In Seattle, this risk is slightly higher (factor of 1.05) than the risk of collapse of equivalently-designed buildings in Los Angeles; in Portland, the risk is a bit lower (factor of 0.81). When the collapse risk is deaggregated by source for the modern buildings in Portland, subduction shaking contributes on average about 88% of the collapse risk. In Seattle, subduction shaking contributes about 79%. The risk of collapse for older RC frames is 7.1 and 7.6 times larger in Portland and Seattle than the modern frames, indicating the well-known higher risk of older concrete buildings. However, these buildings do not appear to be as sensitive to the characteristics of subduction earthquake shaking.

Third, these findings clearly show that seismic performance assessments in which building collapse fragility is quantified based only on crustal motions may substantially underestimate the seismic risk in regions with a subduction hazard. This observation can be used to inform the design of newer buildings by implying a need to considering modifying the design MCE_R values to account for collapse risk from subduction earthquakes.

In addition, the study explored the use of simulated ground motions in nonlinear time history analysis to make up for the limited number of recordings from subduction events. The results show that the simulated ground motions were generally more harmful for structural response than the recorded subduction or crustal ground motions. This difference is attributed to the longer period spectral content of the simulated motions and longer durations than those of the recorded subduction earthquake ground motions. However, the simulated ground motions employed here have not validated against more recently recorded large interface subduction earthquakes in Chile and Japan.

Although the findings of this study focus on RC moment resisting frames, Chandramohan *et al.* (2013) recently showed that steel buildings show similar sensitivity to ground motion duration. This observation is critical since the importance of subduction ground motions is largely linked to ground motion duration effects. Therefore, it is possible to hypothesize that other types of buildings will also have an elevated collapse risk in the Pacific Northwest. This hypothesis may be investigated in future study. Future studies would also benefit from either improved spectral shape factors for subduction ground motions or seismic hazard defined in terms of S_{di} .

8. Acknowledgements

The authors would also like to thank Steve Harmsen, for separating the seismic hazard by subduction and crustal sources, and for providing results from ground motion prediction equations for subduction and crustal earthquakes. The authors also thank Art Frankel for his review of the manuscript and Casey Casias for her input to the study.

9. References

- Abrahamson, N., Gregor, N., and Addo, K. (2012). "BCHydro ground motion prediction equations for subduction earthquakes." *Earthquake Spectra* (submitted).
- American Concrete Institute (ACI). (2008). *Building code requirements for structural concrete (ACI 318-08)*, Farmington Hills, MI.

- ASCE. (2010). *Minimum Design Loads for Buildings and Other Structures (7-10)*, Reston, VA.
- Atkinson, G. M., and Boore, D. M. (2003). "Empirical ground-motion relations for subduction-zone earthquakes and their application to Cascadia and other regions." *Bulletin of the Seismological Society of America*, 93(4), 1703–29.
- Atkinson, G. M., and Macias, M. (2009). "Predicted ground motions for great interface earthquakes in the Cascadia subduction zone." *Bulletin of the Seismological Society of America*, 99(3), 1552–78.
- Baker, J. W. (2007). "Quantitative classification of near-fault ground motions using wavelet analysis." *Bulletin of the Seismological Society of America*, 97(5), 1486.
- Baker, J. W., and Cornell, C. A. (2006). "Spectral shape, epsilon and record selection." *Earthquake Engineering & Structural Dynamics*, 35(9), 1077–1095.
- Baradaran Shoraka, M. (2013). "Collapse assessment of concrete buildings : an application to non-ductile reinforced concrete moment frames." Ph.D Dissertation, University of British Columbia.
- Baradaran Shoraka, M., and Elwood, K. J. (2013). "Mechanical Model for Non Ductile Reinforced Concrete Columns." *Journal of Earthquake Engineering*, 17(7), 937–957.
- Beck, J. L., and Hall, J. F. (1986). "Factors contributing to the catastrophe in Mexico City during the earthquake of September 19, 1985." *Geophysical Research Letters*, 13(6), 593–596.
- Bommer, J. J., and Martínez-Pereira, A. (1999). "The effective duration of earthquake strong motion." *Journal of Earthquake Engineering*, 3(2), 127–172.
- Bommer, J. J., Stafford, P. J., and Alarcón, J. E. (2009). "Empirical equations for the prediction of the significant, bracketed, and uniform duration of earthquake ground motion." *Bulletin of the Seismological Society of America*, 99(6), 3217–33.
- Boore, D. M., and Bommer, J. J. (2005). "Processing of strong-motion accelerograms: needs, options and consequences." *Soil Dynamics and Earthquake Engineering*, 25(2), 93–115.
- CESMD. (2012). "Center for Engineering Strong Motion Data." <http://www.strongmotioncenter.org/>.
- Champion, C., and Liel, A. (2012). "The effect of near-fault directivity on building seismic collapse risk." *Earthquake Engineering & Structural Dynamics*, 41(10), 1391–1409.
- Chandramohan, R., Lin, T., Baker, J. W., and Deierlein, G. G. (2013). "Influence of Ground Motion Spectral Shape and Duration on Seismic Collapse Risk." *10th International Conference on Urban Earthquake Engineering*.
- Cordova, P. P., Deierlein, G. G., Mehanny, S. S., and Cornell, C. A. (2000). "Development of a two-parameter seismic intensity measure and probabilistic assessment procedure." *Proceedings of the 2nd US-Japan Workshop on Performance-Based Seismic Design Methodology for Reinforced Concrete Building Structures, PEER Report*.
- Cornell, C. A. (1968). "Engineering seismic risk analysis." *Bulletin of the Seismological Society of America*, 58(5), 1583–1606.
- Don, L. (2007). "Statewide seismic needs assessment: implementation of Oregon 2005 senate bill 2 relating to public safety, earthquakes, and seismic rehabilitation of public buildings."
- EERI, EMD (WA). (2005). *Scenario for a Magnitude 6.7 Earthquake on the Seattle Fault Earthquake Engineering Research Institute and the Washington Military Department Emergency Management Division June*. 162.

- Elwood, K. J. (2004). "Modelling failures in existing reinforced concrete columns." *Canadian Journal of Civil Engineering*, 31(5), 846–859.
- FEMA. (2009). "Quantification of Building Seismic Performance Factors FEMA P695."
- Frankel, A. D., Carver, D. L., and Williams, R. A. (2002). "Nonlinear and Linear Site Response and Basin Effects in Seattle for the M 6.8 Nisqually, Washington, Earthquake." *Bulletin of the Seismological Society of America*, 92(6), 2090–2109.
- Ghofrani, H., Atkinson, G. M., Goda, K., and Assatourians, K. (2013). "Stochastic Finite-Fault Simulations of the 2011 Tohoku, Japan, Earthquake." *Bulletin of the Seismological Society of America*, 103(2B), 1307–1320.
- Government of Canada. (2012). "Census of Canada." <http://www12.statcan.gc.ca/census-recensement/index-eng.cfm>.
- Hancock, J., and Bommer, J. J. (2006). "A State-of-Knowledge Review of the Influence of Strong-Motion Duration on Structural Damage." *Earthquake Spectra*, 22(3), 827.
- Harmsen, S. (2012). "Personal Communication."
- Haselton, C. B., Liel, A. B., Deierlein, G. G., Dean, B. S., and Chou, J. H. (2011). "Seismic Collapse Safety of Reinforced Concrete Buildings. I: Assessment of Ductile Moment Frames." *Journal of Structural Engineering*, 137, 481.
- Haselton, C. B., Baker, J. W., Liel, A. B., and Deierlein, G. G. (2011b). "Accounting for Ground Motion Spectral Shape Characteristics in Structural Collapse Assessment through an Adjustment for Epsilon." *Journal of Structural Engineering*, 137(3), 332–344.
- Haselton, C. B., Liel, A. B., Lange, S. T., and Deierlein, G. G. (2008). *PEER Report 2007/03 Beam-Column Element Model Calibrated for Predicting Flexural Response Leading to Global Collapse of RC Frame Buildings*.
- Heaton, T. H., and Kanamori, H. (1984). "Seismic potential associated with subduction in the northwestern United States." *Bulletin of the Seismological Society of America*, 74(3), 933–941.
- Ibarra, L. F., Medina, R. A., and Krawinkler, H. (2005). "Hysteretic models that incorporate strength and stiffness deterioration." *Earthquake Engineering & Structural Dynamics*, 34(12), 1489–1511.
- International Conf. of Building Officials (ICBO). (1967). *Uniform Building Code*, Pasadena, CA.
- International Conf. of Building Officials (ICBO). (1973). *Uniform Building Code*, Pasadena, CA.
- International Conf. of Building Officials (ICBO). (1994). *Uniform Building Code*, Pasadena, CA.
- International Code Council (ICC). (2012). *International Building Code*. Falls Church, VA
- K-NET. (2012). "Kyoshin Network K-NET, Strong-Motion Seismograph Network." <http://www.k-net.bosai.go.jp/> (Jun. 17, 2012).
- Kramer, S. L. (1996). *Geotechnical Earthquake Engineering*. Prentice Hall.
- Leyendecker, E.V., Hunt, J.R., Frankel, A.D., and Rukstales, K.S. (2000), "Development of Maximum Considered Earthquake Ground Motion Maps," *Earthquake Spectra*, 16(1), 21-40.
- Liel, A. B., and Deierlein, G. G. (2012). "Using Collapse Risk Assessments to Inform Seismic Safety Policy for Older Concrete Buildings." *Earthquake Spectra*, 28(4), 1495–1521.

- Luco, N., Ellingwood, B. R., Hamburger, R. O., Hooper, J. D., Kimball, J. K., and Kircher, C. A. (2007). "Risk-targeted versus current seismic design maps for the conterminous United States." *Structural Engineers Association of California*, 163–175.
- Mahsuli, M., and Haukaas, T. (2013). "Seismic risk analysis with reliability methods, part II: Analysis." *Structural Safety*, 42, 63–74.
- Mavroeidis, G. P., Zhang, B., Dong, G., Papageorgiou, A. S., Dutta, U., and Biswas, N. N. (2008). "Estimation of Strong Ground Motion from the Great 1964 Mw 9.2 Prince William Sound, Alaska, Earthquake." *Bulletin of the Seismological Society of America*, 98(5), 2303–2324.
- Moehle, J. (1998). "Existing Reinforced Concrete Building Construction." *SEAONC Fall Seminar*.
- Muto, M., and Krishnan, S. (2011). "Hope for the Best, Prepare for the Worst: Response of Tall Steel Buildings to the ShakeOut Scenario Earthquake." *Earthquake Spectra*, 27(2), 375–398.
- NOAA. (2012). "Earthquake Strong Motion Database | National Geophysical Data Center." <http://www.ngdc.noaa.gov/hazard/strong.shtml>.
- OpenSees. (2012). "Open System for Earthquake Engineering Simulation - Home Page." <http://opensees.berkeley.edu/>.
- OSSPAC. (2013). *The Oregon Resilience Plan: Reducing Risk and Improving Recovery for the Next Cascadia Earthquake and Tsunami-Report to the 77th Legislative Assembly from Oregon Seismic Safety Policy Advisory Commission*.
- Pacific Northwest Seismic Network. (2012). "Cascadia Subduction Zone | Pacific Northwest Seismic Network." <http://www.pnsn.org/outreach/earthquakesources/csz>.
- PEER. (2012). "PEER NGA Database." <http://peer.berkeley.edu/nga/>.
- Raghunandan, M. (2013). "Influence of Long Duration Ground Shaking on Collapse of Reinforced Concrete Structures." Ph.D Thesis, University of Colorado at Boulder.
- Raghunandan, M., and Liel, A. B. (2013). "Effect of ground motion duration on earthquake-induced structural collapse." *Structural Safety*, 41, 119–133.
- SeismoSoft. (2012). "SeismoSignal." <http://www.seismosoft.com/en/SeismoSignal.aspx>.
- Sezen, H., and Moehle, J. (2004). "Shear Strength Model for Lightly Reinforced Concrete Columns." *Journal of Structural Engineering*, 130(11), 1692–1703.
- Sørensen, M. B., Atakan, K., and Pulido, N. (2007). "Simulated Strong Ground Motions for the Great M 9.3 Sumatra–Andaman Earthquake of 26 December 2004." *Bulletin of the Seismological Society of America*, 97(1A), S139–S151.
- Tothong, P., and Luco, N. (2007). "Probabilistic seismic demand analysis using advanced ground motion intensity measures." *Earthquake Engineering & Structural Dynamics*, 36(13), 1837–1860.
- US Census. (2012). "Census Bureau Homepage." <http://www.census.gov/>.
- USGS. (2012a). "United States Geological Survey." <http://www.usgs.gov/>.
- USGS. (2012b). "USGS National Strong-Motion Project." <http://nsmp.wr.usgs.gov/>.
- Vamvatsikos, D., and Cornell, C. A. (2002). "Incremental dynamic analysis." *Earthquake Engineering & Structural Dynamics*, 31(3), 491–514.

- White, T., and Ventura, C. E. (2004). "Ground motion sensitivity of a Vancouver-style high rise." *Canadian Journal of Civil Engineering*, 31(2), 292–307.
- Yang, J. (2009). "Nonlinear Responses of High-Rise Buildings in Giant Subduction Earthquakes." Ph.D Thesis, California Institute of Technology.
- Zhao, J. X. (2006). "Attenuation Relations of Strong Ground Motion in Japan Using Site Classification Based on Predominant Period." *Bulletin of the Seismological Society of America*, 96(3), 898–913.